



Circuits and Systems

Mekelweg 4,
2628 CD Delft
The Netherlands

<http://ens.ewi.tudelft.nl/>

CAS-2013-00

M.Sc. Thesis

Space-varying FIR filter design for nonuniformly sampled seismic data

Apostolos Kontakis B.Sc.

Abstract

Since the early days of exploration seismology seismic receiver field arrays have been employed for purposes such as suppressing high wavenumbers present in wavefield, reducing the volume of recorded data and improving its signal-to-noise ratio. These receiver field arrays rely on the receivers being placed on a predetermined geometric layout, a condition which is not always met in the field. Misplacing receivers can have a detrimental effect on the performance of the field array. Fortunately, advances in seismic acquisition now enable a) recording the output of individual receivers and b) knowing with high (but limited) accuracy the actual location of each receiver. It is possible then to form arrays digitally on a computer, a process known as group forming. Group forming can be viewed as a combination of filtering and resampling. We propose two algorithms that take advantage of the positional information available about the receivers and generate a linear space-varying (LSV) filter. The LSV filter is suitable for filtering the nonuniformly sampled data, generating the filtered output on the nominal grid. We examine the relation of our algorithms with other algorithms from the bibliography and investigate their performance on synthetic data.

Space-varying FIR filter design for nonuniformly sampled seismic data

THESIS

submitted in partial fulfillment of the
requirements for the degree of

MASTER OF SCIENCE

in

ELECTRICAL ENGINEERING

by

Apostolos Kontakis B.Sc.
born in Athens, Greece

This work was performed in:

Novel Geophysical Measurements (PTI/EN)
Shell Global Solutions International B.V.
Kessler Park 1, 2288 GS, Rijswijk, The Netherlands



Delft University of Technology

Copyright © 2013 Circuits and Systems Group
All rights reserved.

DELFT UNIVERSITY OF TECHNOLOGY
DEPARTMENT OF
TELECOMMUNICATIONS

The undersigned hereby certify that they have read and recommend to the Faculty of Electrical Engineering, Mathematics and Computer Science for acceptance a thesis entitled “**Space-varying FIR filter design for nonuniformly sampled seismic data**” by **Apostolos Kontakis B.Sc.** in partial fulfillment of the requirements for the degree of **Master of Science**.

Dated: 4-3-2013

Chairman:

Prof.dr.ir. Geert Leus

Advisor:

Dr.ir. Xander Campman

Committee Members:

Prof.dr.ir. Geert Leus

Prof.dr.ir. Dries Gisolf

Dr.ir. Xander Campman

Abstract

Since the early days of exploration seismology seismic receiver field arrays have been employed for purposes such as suppressing high wavenumbers present in wavefield, reducing the volume of recorded data and improving its signal-to-noise ratio. These receiver field arrays rely on the receivers being placed on a predetermined geometric layout, a condition which is not always met in the field. Misplacing receivers can have a detrimental effect on the performance of the field array. Fortunately, advances in seismic acquisition now enable a) recording the output of individual receivers and b) knowing with high (but limited) accuracy the actual location of each receiver. It is possible then to form arrays digitally on a computer, a process known as group forming. Group forming can be viewed as a combination of filtering and resampling. We propose two algorithms that take advantage of the positional information available about the receivers and generate a linear space-varying (LSV) filter. The LSV filter is suitable for filtering the nonuniformly sampled data, generating the filtered output on the nominal grid. We examine the relation of our algorithms with other algorithms from the bibliography and investigate their performance on synthetic data.

Acknowledgments

I would like to thank a number of people, whose help and guidance proved to be invaluable. First of all, I would like to like to thank Dr. Xander Campman, both for trusting me to undertake this project and for his daily supervision. His advice and experience proved to be the best weapon against the stumbling blocks that will invariably occur.

I would also like to thank Prof. Geert Leus for his precious assistance in shaping a solution that satisfied the goals of the project. Our discussions helped me identify potential pitfalls and were a tremendous aid.

This note would be incomplete without the names of Zijian Tang and Mike Danilouchkine, who always tirelessly offered help and advice. For this I thank them dearly. Finally, I would like to thank Prof. Dries Gisolf for accepting to participate in my thesis committee.

Apostolos Kontakis B.Sc.
Delft, The Netherlands
4-3-2013

Contents

Abstract	v
Acknowledgments	vii
1 Introduction	1
1.1 Problem statement	2
1.2 Thesis organization	2
1.3 Notation	4
1.3.1 Unary and binary operations on matrices	4
1.3.2 Functions of vectors and matrices	5
2 Sampling the wavefield	7
2.1 The sampling grids	7
2.2 Apparent velocities and the FK spectrum	9
2.3 The spatial sampling interval	10
3 Group forming	13
3.1 Filtering	14
3.1.1 Uniform input grid	14
3.1.2 Nonuniform input grid	15
3.2 Resampling	16
4 The effects of nonuniform sampling on the spectrum	17
4.1 Deterministic sampling	17
4.2 Stochastic sampling	19
5 Group forming for nonuniformly sampled data	23
5.1 The one-dimensional case	23
5.1.1 Spatial domain optimization	23
5.1.2 Wavenumber domain optimization	26
5.2 The two-dimensional case	28
5.2.1 Spatial domain optimization	28
5.2.2 Wavenumber domain optimization	30
5.3 Geometry compensating digital group forming	32
5.3.1 The two-dimensional case	32
5.3.2 The one-dimensional case	35
5.4 Comparison of methods and related discussion	35
6 Results	39
6.1 Experimental setup: one-dimensional case	39
6.1.1 Acquisition geometry and velocity model	39
6.1.2 Source wavelet	39

6.1.3	Filtering and decimation	39
6.1.4	Results - one spatial dimension	41
6.2	Experimental setup: two-dimensional case	43
6.2.1	Acquisition geometry	44
6.2.2	Generating the data	44
6.2.3	Filtering and decimation	46
6.2.4	Results - two spatial dimensions	46
7	Conclusions and suggestions for future work	53
A	Appendix	55
A.1	The sincd() function	55

Introduction

Over the years, exploration geophysics has utilized a multitude of methods in order to probe the composition and structure of the first few kilometers of the Earth. Reflection seismology is one such method. Back in 1921 it was experimentally shown for the first time that subsurface layers of the Earth can be mapped using a dynamite charge to generate a seismic wave and seismograms to record the reflected wavefronts[6]. Today, very similar techniques are routinely used in subsurface exploration and especially in the search for underground areas likely to contain hydrocarbons.

Reflection seismology exploits the properties of elastic wave propagation in matter. In the most simple case, seismic sources generate seismic waves that propagate through the Earth's interior layers (body waves), on the Earth's surface (surface waves) and in the air (air waves). When the body waves meet an interface between two different layers, part of their energy is reflected and part of it is refracted into the next layer. A portion of the wavefield's energy returns to the surface of the Earth where it is captured by specialized receivers, called geophones or hydrophones depending on whether they operate on land or in water. A simplified schematic of this scenario can be seen in Figure 1.1. The output of these receivers provides a spatially sampled version of the continuous seismic wavefield in time. There are, however, two main reasons why traditionally the output of individual receivers is rarely used directly: poor signal to noise ratio (SNR) and storage/computational costs. With the modern capabilities of digital storage and processing power, recording the output of every individual receiver is possible, even when tens or hundreds of thousands of receivers are deployed. The problem of improving the quality of the signal still remains though.

Traditionally these problems have been attacked by grouping receivers and summing their output in the field, by connecting all group outputs together. The grouped receivers are usually referred to as a field array of receivers and the process as group forming. The resulting signal has an improved signal to noise ratio (SNR) and the high-wavenumber content is suppressed. The quantity of data that has to be stored for further use is also reduced. The SNR is thus improved and storage/processing demands remain at reasonable levels, when this is needed. Further, such types of data pre-processing (e.g. suppression of incoherent noise) may be needed by some imaging algorithms.

Harnessing the advantages of a field array, presupposes that the receivers will be placed at specific locations, determined when designing the array. Failure to do so may have detrimental effects on the performance of the array. In this thesis, we will primarily deal with the effects of receiver positioning deviations and potential group forming methods that compensate for positional deviations.

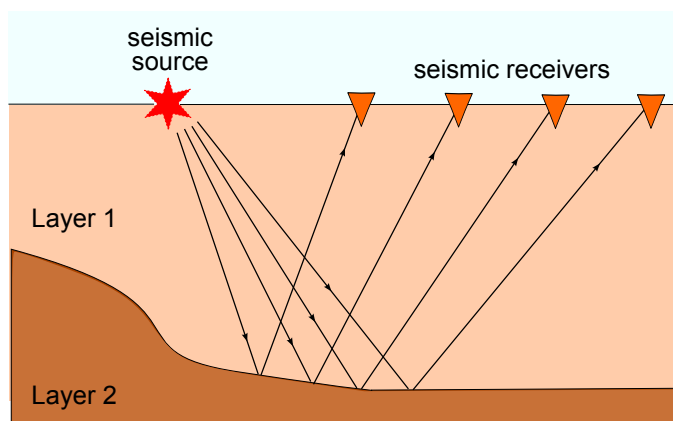


Figure 1.1: A simplified version of seismic exploration.

1.1 Problem statement

The main objective of this thesis is to develop methods to perform group forming that take into account deviations from nominal positions in receiver locations. These methods use knowledge about the actual locations of the deployed receivers and should be robust. Robustness here means that different realizations of the receiver locations should affect as little as possible the output after group forming. This output should be as close as possible to the ideal output which is obtained when the receivers have zero deviation from the nominal location.

1.2 Thesis organization

This thesis is organized as follows:

Chapter 2 establishes the geometry of the receiver layout that will be assumed throughout this thesis. The concept of the apparent velocity and its relation to the frequency-wavenumber spectrum is introduced. The notion of adequate sampling is discussed as well.

Chapter 3 introduces the concept of group forming in more detail and gives an overview of various approaches that have been proposed over the years. Two different cases are distinguished, depending on whether deviations from the underlying (nominal) grid can exist or not.

Chapter 4 discusses the effects of nonuniform sampling to the spectral content of the data and demonstrates the necessity to take this effect into account.

Chapter 5 presents two methods that we propose for group forming for nonuniform grids. We also present in detail geometry compensating digital group forming, a method that has been previously proposed and which will be used for benchmarking purposes in the next section. In the end of the section a comparison with other methods in the bibliography is given.

Chapter 6 contains the results of the application of the two proposed methods on synthetic data. Two benchmarks are used for comparison: group forming ignoring the irregularities in sampling and the geometry compensating digital group forming algorithm.

1.3 Notation

Throughout this work several notational conventions will be followed. These are listed below.

ι : The imaginary unit $\iota = \sqrt{-1}$.

\mathbf{v} : Vectors will be written as boldface lower case letters.

\mathbf{A} : Matrices will be denoted with boldface capital letters.

$\mathbf{A}_{N \times M}$: \mathbf{A} has N rows and M columns.

1.3.1 Unary and binary operations on matrices

A number of unary and binary operations on matrices are frequently used. Let

$$\mathbf{A} = \begin{bmatrix} A_{1,1} & \cdots & A_{0,M_A} \\ \vdots & & \vdots \\ A_{N_A,0} & \cdots & A_{N_A,M_A} \end{bmatrix}_{N_A \times M_A} \quad \text{and} \quad \mathbf{B} = \begin{bmatrix} B_{1,1} & \cdots & B_{0,M_B} \\ \vdots & & \vdots \\ B_{N_B,0} & \cdots & B_{N_B,M_B} \end{bmatrix}_{N_B \times M_B}.$$

Then, the following notation is introduced:

\mathbf{A}^* : The complex conjugate of \mathbf{A} .

\mathbf{A}^T : The transpose of \mathbf{A} .

\mathbf{A}^H : The Hermitian (complex conjugate) transpose of \mathbf{A} .

\mathbf{A}^\dagger : The left Moore-Penrose pseudoinverse of \mathbf{A} when \mathbf{A} has full column rank is given by $\mathbf{A}^\dagger = (\mathbf{A}^H \mathbf{A})^{-1} \mathbf{A}^H$.

$\|\mathbf{A}\|_F$: The Frobenius norm of \mathbf{A} , given by

$$\|\mathbf{A}\|_F = \sqrt{\sum_{i=1}^{N_A} \sum_{j=1}^{M_A} A_{i,j}^2}.$$

$\mathbf{A} \odot \mathbf{B}$: The Hadamard (elementwise) product of \mathbf{A} and \mathbf{B} . This is defined when $N_A = N_B$ and $M_A = M_B$ as

$$\mathbf{A} \odot \mathbf{B} = \begin{bmatrix} A_{1,1}B_{1,1} & \cdots & A_{0,M_A}B_{0,M_B} \\ \vdots & & \vdots \\ A_{N_A,0}B_{N_B,0} & \cdots & A_{N_A,M_A}B_{N_B,M_B} \end{bmatrix}_{N_A \times M_B}.$$

$\mathbf{A} \otimes \mathbf{B}$: The Kronecker product of \mathbf{A} and \mathbf{B} , defined as

$$\mathbf{A} \otimes \mathbf{B} = \begin{bmatrix} A_{1,1}\mathbf{B} & \cdots & A_{0,M_A}\mathbf{B} \\ \vdots & & \vdots \\ A_{N_A,0}\mathbf{B} & \cdots & A_{N_A,M_A}\mathbf{B} \end{bmatrix}_{N_A N_B \times M_A M_B}.$$

1.3.2 Functions of vectors and matrices

Let

$$\mathbf{A} = \begin{bmatrix} A_{1,1} & \cdots & A_{0,M_A} \\ \vdots & & \vdots \\ A_{N_A,0} & \cdots & A_{N_A,M_A} \end{bmatrix}_{N_A \times M_A} \quad \text{and} \quad \mathbf{v} = \begin{bmatrix} v_1 \\ v_2 \\ \vdots \\ v_N \end{bmatrix}_{N \times 1}.$$

Then the following functions can be defined.

$\text{row}(\mathbf{A}; l)$: The l 'th row of \mathbf{A} ,

$$\text{row}(\mathbf{A}; l) = [A_{l,1}, A_{l,2}, \dots, A_{l,M_A}]_{1 \times M_A}.$$

$\text{diag}(\mathbf{v})$: The diagonal matrix with the elements of \mathbf{v} on its diagonal,

$$\text{diag}(\mathbf{v}) = \begin{bmatrix} v_1 & 0 & \cdots & 0 \\ 0 & v_2 & \ddots & \vdots \\ \vdots & \ddots & \ddots & 0 \\ 0 & \cdots & 0 & v_N \end{bmatrix}_{N \times N}.$$

$\text{vec}(\mathbf{A})$: The vector constructed by stacking each column of \mathbf{A} one below the other,

$$\text{vec}(\mathbf{A}) = \begin{bmatrix} A_{1,1} \\ A_{2,1} \\ \vdots \\ A_{N_A,1} \\ A_{1,2} \\ \vdots \\ A_{N_A,M_A} \end{bmatrix}_{N_A M_A \times 1}.$$

$\text{circ}(\mathbf{v})$: The circulant matrix with \mathbf{v} as the first column; the rest of the columns are cyclic permutations of the first one,

$$\text{circ}(\mathbf{v}) = \begin{bmatrix} v_1 & v_N & \cdots & v_3 & v_2 \\ v_2 & v_1 & v_N & & v_3 \\ \vdots & v_2 & v_1 & \ddots & \vdots \\ v_{N-1} & & \ddots & \ddots & v_N \\ v_N & v_{N-1} & \cdots & v_2 & v_1 \end{bmatrix}_{N \times N}.$$

Sampling the wavefield

2.1 The sampling grids

As was stated in the introduction, special devices known as geophones or hydrophones can record components of the continuous seismic wavefield in space and time. Here we will assume that the receivers measure the z -axis (vertical) component of the particle velocity field. Let

$$d(t, x_s, y_s, z_s, x_r, y_r, z_r) \quad (2.1)$$

be a scalar valued function denoting the value of the vertical particle velocity field. The coordinates (x_s, y_s, z_s) are the coordinates of a seismic source, while (x_r, y_r, z_r) are the coordinates of a receiver¹. Note that in a (2.1) we assume, without loss of generality, that a single source is active each time. The variable t denotes time. The value of the particle velocity field versus time for a particular combination of source and receiver coordinates is called a seismic trace.

It is very common to select a specific subspace of the 7-dimensional space of (2.1). A specific subspace of the data, commonly known as a panel or gather, may highlight specific characteristics of the recorded wavefield. Examples of panels include the Common Shot Panel (CSP), which is the (t, x_r, y_r, z_r) subspace, the Common Receiver Panel, which is the (t, x_s, y_s, z_s) subspace. The algorithms proposed in this work may be applied to any of the possible two-dimensional subspaces. For simplicity we assume a CSP where the two dimensions map to $(x_r, y_r, 0) \equiv (x, y)$ and the value of the vertical particle velocity field is given by

$$d(x, y), \quad (2.2)$$

Similarly, in the one-dimensional case, we assume that the receivers lie on the x -axis. Then, (2.2) simply becomes $d(x)$.

Some further assumptions are made regarding the placement of the receivers in the field. In order to facilitate the discussion of these assumptions we define four types of receiver grids, which are also depicted in Fig. 2.1.

- The **input** grid: This grid is defined by the actual locations of the geophones. The coordinates of the geophones are the set $\{x_i\}$ when the geophones are placed on a line and $\{(x_i, y_j)\}$ when they are placed on a plane.
- The **nominal grid**: The nominal grid is a rectangular grid with uniform spacings. The spacings, which define the nominal sampling interval, are Δx along the x -axis and Δy along the y -axis. Ideally the receivers should be placed on the nodes of the nominal grid, however this is not always the case in practical situations.

¹An alternative to using the source-receiver coordinates as in (2.1) is to use the midpoint-offset coordinates [18, Chapter 3].

- The **output** grid: This grid is defined by the set of group forming output coordinates. Unless specified otherwise, we assume that the output grid will be a subset of the nominal grid defined above.
- The **dense grid**: When the receivers are distributed on a line, this will be a uniform grid with spacing δx . When the receivers are distributed on a plane it will be a regular grid with uniform spacings $\delta x = \frac{1}{M_x}\Delta x$ and $\delta y = \frac{1}{M_y}\Delta y$. M_x and M_y are integers greater or equal to 1.

More often than not, the input grid will not be a subset of the dense grid. In this case we assume that the traces are collected at the closest dense grid point instead, since in reality the location of each receiver is known with limited accuracy anyway. M_x and M_y are chosen such that δx and δy are less or equal to the accuracy of the receiver location measurement.

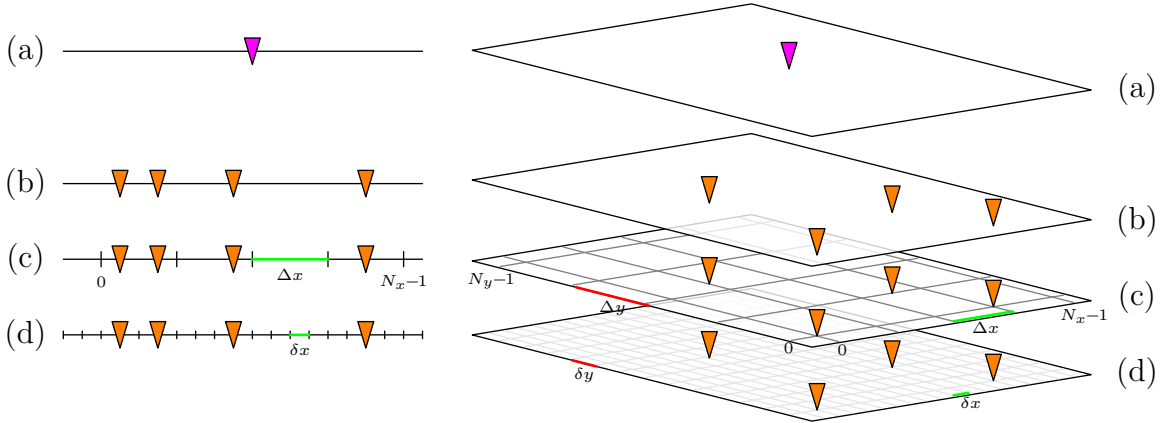


Figure 2.1: The same set of receivers projected on (b) the input grid, (c) the nominal grid and (d) the dense grid. Their weighted and summed outputs generates the result on the output grid (a). Here $N_x = 5$, $N_y = 5$, $M_x = 4$ and $M_y = 3$. For clarity, not all receivers are shown.

The actual receiver coordinates can be written as the coordinates of the nominal grid plus their deviations from their nominal location:

$$\begin{aligned} x_i &= \bar{x}_i + \delta x_i && \text{for the one-dimensional case,} \\ (x_i, y_j) &= (\bar{x}_i, \bar{y}_j) + (\delta x_{i,j}, \delta y_{i,j}) && \text{for the two-dimensional case.} \end{aligned} \quad (2.3)$$

A single bar denotes a coordinate component on the nominal grid, i.e. $\bar{x}_i = i\Delta x$ and $\bar{y}_j = j\Delta y$. Similarly, a double bar denotes a coordinate component defined on the dense grid, i.e. $\bar{\bar{x}}_i = i\delta x$ and $\bar{\bar{y}}_j = j\delta y$.

Occasionally in this work there is a need for indicator functions that are only nonzero at the coordinates where receivers are present. We introduce two such functions, $s_\delta(\cdot)$ for the continuous-space case and its discrete counterpart $s(\cdot)$ which is defined on the

dense grid:

$$s_\delta(x) = \sum_i \delta(x - x_i),$$

$$s(x) = \begin{cases} 1 & \text{if } x = \bar{x}_i \text{ and there is a receiver present at } \bar{x}_i \\ 0 & \text{otherwise} \end{cases}$$

where $\delta(\cdot)$ is the Dirac delta distribution. For the two-dimensional case we have

$$s_\delta(x, y) = \sum_i \sum_j \delta(x - x_i, y - y_j)$$

$$s(x, y) = \begin{cases} 1 & \text{if } x = \bar{x}_i, y = \bar{y}_j \text{ and there is a receiver present at } (\bar{x}_i, \bar{y}_j) \\ 0 & \text{otherwise.} \end{cases}$$

2.2 Apparent velocities and the FK spectrum

The data is sampled in time and space, however the time-space (TX) domain is not always the most intuitive representation of the data. A good example of this occurs when one wants to discriminate between different kinds of waves, based on their velocity, angle of arrival and frequency content. Knowledge of these parameters enables us to characterize the composition of the sampled wavefield energy in terms of wave types such as direct waves, reflections, multiples etc. It also makes filtering out specific wave types much easier.

The Fourier transform is an important tool that can be used for this purpose. The temporal and spatial transformation from the TX domain to the frequency-wavenumber²(FK) domain can be used to differentiate waves based on their apparent velocities.

Let us assume a line of receivers, equispaced along the x -axis. This setup is known as a uniform linear array and appears often in radar and communications as well. The apparent velocity of a wave is the velocity it appears to have along the line of receivers. A schematic representation can be seen in Fig. 2.2. For simplicity, we will assume a plane

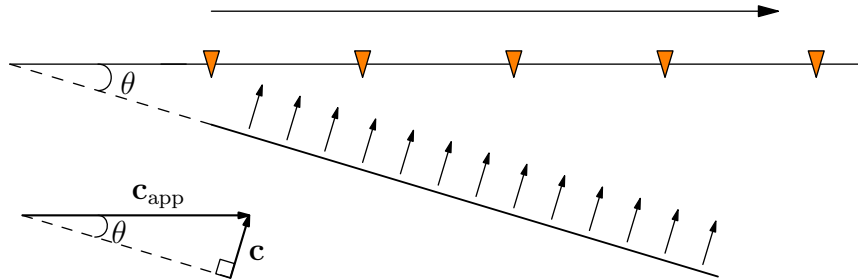


Figure 2.2: A plane wave arriving at an angle θ having velocity \mathbf{c} .

²Sometimes the term “spatial frequency” is used in the literature instead of the term “wavenumber”.

wave arriving with velocity \mathbf{c} and frequency f impinging on the receivers with an angle θ . Then the apparent velocity is given by

$$\|\mathbf{c}_{\text{app}}\|_2 = \frac{\|\mathbf{c}\|_2}{\sin(\theta)}$$

The apparent wavelength and the apparent velocity are linked via the frequency of the wave

$$\|\mathbf{c}_{\text{app}}\|_2 = \lambda_{\text{app}} f,$$

where λ_{app} is the apparent wavelength. A special case arises when the wavefront is parallel to the x -axis. Then the apparent wavelength will be infinity. The reciprocal of the apparent wavelength is the apparent wavenumber

$$k_{\text{app}} = \frac{1}{\lambda_{\text{app}}} = \frac{f}{\|\mathbf{c}_{\text{app}}\|_2}. \quad (2.4)$$

The apparent wavenumber is linked in a linear manner with frequency, assuming no dispersion. It can be seen that in an FK spectral plot, any straight line passing through the origin will represent a constant apparent velocity. Ground roll travels near the surface of the Earth, generally with lower apparent velocities than the reflections coming from underneath. Provided that no aliasing occurs, ground roll energy and reflection energy generally occupy distinct areas in the FK spectrum of the data. An example is demonstrated in Fig. 2.3. For simplicity, in the following sections apparent wavenumber should be understood whenever the word wavenumber is mentioned. The reflected energy will generally be near $k = 0m^{-1}$, since its wavefronts will generally arrive at an angle close $\theta = 0$ i.e., almost parallel to the axis (or plane) of the receivers. The apparent velocity of those wavefronts will be very large and it can be seen from (2.4) that the apparent velocity will be close to 0.

2.3 The spatial sampling interval

In order to have an alias-free recorded wavefield, according to the sampling theorem, the spatial sampling rate k_{smp} should be no less than the twice the largest wavenumber present in the wavefield, k_{max} .

$$k_{\text{smp}} \geq 2k_{\text{max}}.$$

This means that the sampling interval $\Delta x = 1/k_{\text{smp}}$ should be

$$\Delta x \leq \frac{1}{2}\lambda_{\text{min}},$$

or in other words, that at least two samples should be acquired per minimum apparent wavelength. If this condition is not met, than some of the recorded bandwidth will be contaminated by aliases of the high wavenumbers. A more detailed explanation for this phenomenon can be found in Chapter 4.

Usually the ground roll will have the minimum apparent wavelength as it is usually the wave with the lowest apparent velocity. If we only care about the more narrow-band

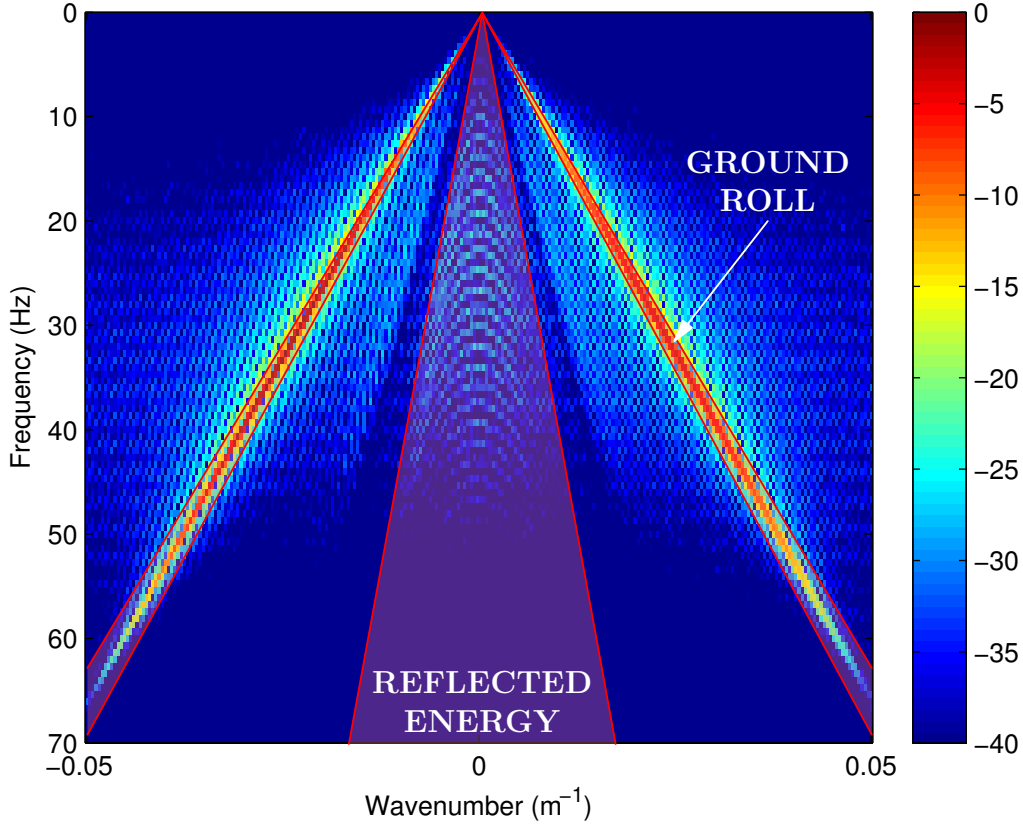


Figure 2.3: Constant apparent velocities appear as straight lines passing through the origin in FK plots. The reflected wave energy can be clearly distinguished from the ground roll which has much lower apparent velocities.

signal that contains only the energy of the reflections, then we can consider the ground roll as part of the noise [18, Chapter 4]. In this situation it is possible to permit some aliasing of the ground roll, by increasing Δx . This is possible when single receivers are used for acquisition and can lead to cost savings during a survey because less receivers have to be used to cover a particular area [1]. The condition that should be met is that the aliased wavenumbers should not enter the region of the spectrum considered “signal”.

A wavenumber $k \geq k_{\text{smp}}/2$ sampled at sampling rate k_{smp} will be aliased to the wavenumber

$$\frac{k_{\text{smp}}}{2} - \left(k - \frac{k_{\text{smp}}}{2}\right) = k_{\text{smp}} - k$$

A schematic example can be seen in Fig. 2.4. We may sample at rate k_{adq} , instead of k_{smp} , provided that any aliased wavenumber should be higher or equal to the highest wavenumber of the portion of the spectrum that is considered signal. We denote that wavenumber as k_{sig} . Then

$$k_{\text{adq}} - k \geq k_{\text{sig}}, \quad \forall k$$

The highest wavenumber contained in the spectrum is usually the highest wavenumber of the ground roll, k_{gr} . Then the previous inequality becomes

$$k_{adq} \geq k_{sig} + k_{gr}$$

$$\frac{1}{\Delta x_{adq}} \geq \frac{1}{2\Delta x_{sig}} + \frac{1}{2\Delta x_{gr}}$$

$$\Delta x_{adq} \leq \frac{2\Delta x_{sig}\Delta x_{gr}}{\Delta x_{sig} + \Delta x_{gr}},$$

where Δx_{adq} is the adequate sampling interval, Δx_{sig} would be the required sampling interval to record the signal unaliased and Δx_{gr} is the sampling interval that guarantees unaliased sampling of the ground roll. When $\Delta x_{sig} < \Delta x_{gr}$, $\Delta x_{adq} < \Delta x_{gr}$ and therefore the sampling density can be reduced without harming the signal. Sampling with a sampling interval of Δx_{adq} means that the ground roll energy may be aliased, but the aliases will not enter the reflection part of the spectrum.

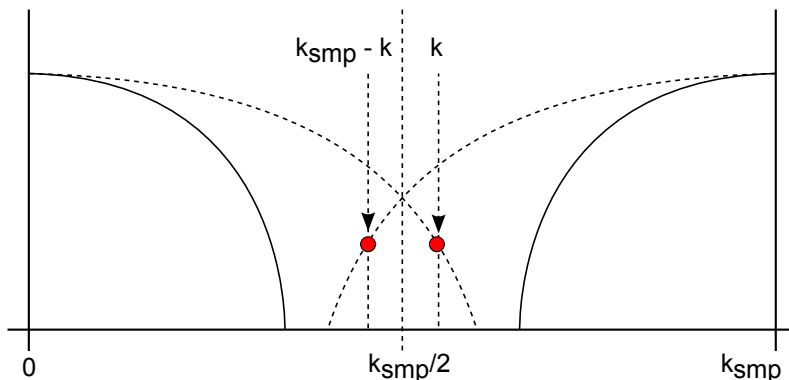


Figure 2.4: A example of wavenumber aliasing. The signal represented by the solid line is sampled above the Nyquist rate. The dashed line represents a signal sampled below the Nyquist rate. A wavenumber $k > k_{smp}/2$ is mapped to $k_{smp}-k$.

3

Group forming

As we previously saw, it is possible to represent the sampled data in a different domain than the domain they were recorded in. By transforming the data to the frequency-wavenumber (FK) domain, it is possible to view the velocities of arriving waves as linear segments. The advantage of this domain of representation is that now signal and noise are much more decoupled. Noise removal can be effectively done by filtering out combinations of frequencies and wavenumbers.

When recording is done in an analog fashion, filtering out frequencies can be performed by passing the signal recorded by the receiver through analog filters with the desired properties. In order to perform a similar type of filtering in the wavenumber domain, one can take advantage of the fact that each wavefront arrives at a different velocities at each receiver. By summing the outputs of a number of receivers it is possible to selectively attenuate waves with certain velocities more than others, hence performing a spatial type of filtering. A set of receivers whose output is summed is commonly termed a field array, a field pattern or a group. A schematic depiction of a group can be seen in Fig. 3.1.

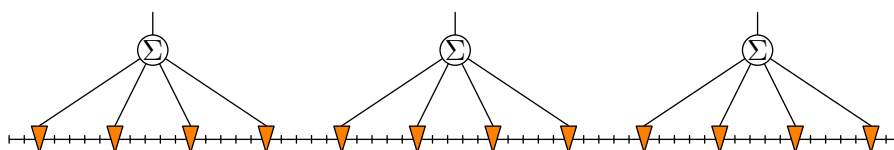


Figure 3.1: Schematic depiction of a receiver group.

Group forming can be done both in the analog and in the digital domain, the difference being whether the summation is performed before recording the receiver (analog group forming) or after (digital group forming). Digital group forming essentially depends on the ability to record single sensors. Recording each receiver output, however, has not always been an option, due to the huge amount of storage and recording capabilities required. Nowadays though, recording each receiver output is technologically feasible and makes it possible to completely separate signal acquisition, done in the field, from signal processing to be done digitally on the computer [13, 1].

Whether done in the analog or the digital domain, group forming can be conceptually seen as a succession of two steps, namely

- filtering, since summing a number of (possibly weighted) receiver outputs can be interpreted as applying a finite impulse response (FIR) filter along the spatial dimensions and
- resampling, since one filter output per group of receivers is kept. When the filter outputs are generated on the nominal grid, resampling takes the form of

decimation. However, other possibilities also exist, such as generating the filter outputs on a denser grid, or even at arbitrary locations [3, 14].

In the following sections we examine some practical considerations concerning these two steps.

3.1 Filtering

The way filtering is conducted can be divided into two classes of methods. The first class assumes that the input grid has some form of regularity, for example that it is a line with uniform spacings or a rectilinear grid. The second class makes no such assumption. When the filter parameters are decided, consideration must be given to the following

1. The filter length should not be very large. A large filter length means that traces which refer to significant variations in the subsurface might be summed. This has the potential of introducing artifacts in the output.
2. The filter should be able to suppress aliasing that would be introduced after the resampling phase. This is discussed in Section 3.2.
3. The actual geometry of the input grid should be taken into account, especially if it deviates significantly from its theoretical description. A discussion on why this can be important can be found in Chapter 4.

It is possible that not all of these considerations can be satisfied at the same time, depending on which group forming is to be used. Usually the first two requirements cannot be satisfied at the same time, because a FIR filter with excellent passband/stop-band characteristics might require a very large number of taps. This, however, is very likely to violate the first condition.

3.1.1 Uniform input grid

The simplest kind of group is composed of L_f identical equidistant receivers with a spacing of Δx and a gain of $\frac{1}{L_f}$ [18]. Its discrete-time Fourier transform is given by

$$H_u(e^{ik}) = \sum_{l=-(L_f-1)/2}^{(L_f-1)/2} \frac{1}{L_f} e^{-i2\pi k \bar{x}_l} = \frac{\sin(\pi k L_f \Delta x)}{L_f \sin(\pi k \Delta x)}$$

If we do the substitution $\Delta x = \Delta X / (L_f - 1)$ where ΔX is the physical length occupied by the L_f receivers, and take the limit as $L_f \rightarrow \infty$ we get

$$\lim_{L_f \rightarrow \infty} H_u(e^{ik}) = \lim_{L_f \rightarrow \infty} \frac{\sin\left(\pi k \frac{L_f}{L_f-1} \Delta X\right)}{L_f \sin\left(\pi k \frac{1}{L_f-1} \Delta X\right)} = \frac{\sin(\pi k \Delta X)}{\pi k \Delta X}$$

which is the cardinal sine (sinc) function, i.e., the Fourier transform of the boxcar function. The continuous variable k denotes the wavenumber in m^{-1} . The final spectrum after convolving the boxcar function with the data, will be a product of the DTFT of the sampled data with $H_u(e^{jk})$. Although convenient due to its simplicity, the uniformly weighted filter has a number of drawbacks, the most important being the inability to influence the amplitude of the sidelobes for a given number of receivers and sampling interval.

A way to have more control over the wavenumber response of the group is to introduce arbitrary gains and inter-receiver spacings on the receivers [16]. Then the wavenumber response becomes

$$H(e^{jk}) = \sum_{l=-(L_f-1)/2}^{(L_f-1)/2} h(x_l) e^{-j2\pi k x_l}.$$

where $h(x_l)$ are the individual gains and x_l the locations of the geophones. There is a plurality of ways to select the gain values, drawing from a vast body of work in filter theory. Savit et al. developed the moveout filter, which approximates an ideal frequency response in the least squares sense, by either optimizing with respect to the inter-receiver spacings or with respect to the receiver gains [16]. The latter case is identical to the usual least squares FIR filter design with the further constraint that the gains are such that the wavenumber response of the filter is 1 for $k = 0$. Chebyshev weights are another option explored in [15, 10]. As Holzman notes, arrays using Chebyshev weights have the narrowest passband lobe for a given absolute upper bound in the stopband region, and conversely, have the the lowest absolute upper bound in the stopband region for a given passband lobe width. The downside of using Chebyshev gains, however, is that their wavenumber response is very sensitive to gain and location variations in the receiver. Using the method proposed in [17], it is possible to design the best possible Chebyshev array with respect to the tolerance of the gain variations. Gain variations are generally an important consideration for any group scheme which uses different weights for its elements. It is especially true if groups are formed in the field and these gains are implemented in the receiver hardware and are thus depending on the tolerances of the electronic circuitry. For the rest of this work we assume that the receivers do not exhibit gain variations.

3.1.2 Nonuniform input grid

The methods outlined in the previous section assume spatial uniformity in the input grid. However in practical situations this is rarely true. Due to obstacles and other terrain difficulties, misplacement of the equipment etc., it is very possible that some of the receivers are not positioned very accurately. The question that arises is how should filtering be performed in this situation, where the filter and the data lie on different grids. Generally three approaches are used to deal with this problem:

1. Regularization¹ of the data and application of a filter designed for the nominal grid.

¹Regularization in the sense of interpolation to the nominal grid.

2. Design of a filter that operates at the input grid rather than at the nominal one.
3. Disregard the fact that the input grid and the nominal grid are different and simply filter the data using a filter designed for the nominal grid.

The approach of [7] is of the first kind. The method introduced there estimates the spectrum of the data using parametric inversion. Then the signal can be reconstructed to the nominal grid by means of a simple inverse FFT. Filtering can then be performed easily on the reconstructed data. A variant of their method that directly reconstructs the data is also included in [7]. We discuss the details of this variant in Section 5.4.

An example of the second approach is the geometry compensating digital group forming method [8]. This method interpolates a predesigned filter to the input grid and applies additional weighting to each filter tap that compensates for the variations in sampling density caused by the irregularities of the input grid. A detailed description of this method is included in Chapter 5.3, as a benchmark for our proposed methods. Among the advantages of this method, as the authors of [8] note, are the fact that it makes no assumption about the characteristics of the data. It is also much less computationally demanding than first regularizing the data and applying the filter afterwards.

3.2 Resampling

Resampling may take place after filtering. In the example of Fig. 3.1, the filter output is decimated with a resampling ratio $\beta = 4$. Decimation can be easily performed if group forming is done digitally, as it merely means that filter outputs do not have to be calculated for every possible spatial shift of the filter. It is possible to have arbitrary resampling ratios, for example with the aid of fractional delay filters.

Since usually resampling is used to reduce the amount of seismic data, $\beta > 1$. The new sampling interval $\Delta x'$ becomes larger than the original sampling interval Δx

$$\Delta x' = \beta \Delta x$$

$$k'_{smp} = \frac{1}{\beta} k_{smp},$$

or equivalently the sampling rate $k'_{smp} = 1/\Delta x'$ becomes β times smaller. Any wavenumber greater than $k'_{smp}/2$ will be aliased in the resampled data. Due to this reason, the filtering should be performed such that wavenumbers that would be aliased are attenuated as much as possible. In essence, the filter should have adequate antialiasing characteristics [3].

The effects of nonuniform sampling on the spectrum

4

4.1 Deterministic sampling

When filtering is to be performed on sampled data, the way the sampling was conducted matters and should be taken into account. This dependence on sampling regularly can be demonstrated with an example. Assume that an infinite number of receivers is distributed along the x -axis at locations x_l for $l = -\infty, \dots, -1, 0, 1, \dots, +\infty$. For simplicity we only consider irregularities in the sampling of the x -axis, assuming that sampling is uniform in the time domain. Let

$$d_s(x) = d(x) \sum_{l=-\infty}^{+\infty} \delta(x - x_l) \quad (4.1)$$

be the sampled version of $d(x)$. With the aid of the comb function $s_\delta(x) = \sum_{l=-\infty}^{+\infty} \delta(x - x_l)$ (4.1) then becomes

$$d_s(x) = d(x)s_\delta(x). \quad (4.2)$$

An important question that arises is what is the relation between the wavenumber spectra of $d_s(x)$ and $d(x)$. Assuming that the Fourier transform¹ pairs

$$d(x) \leftrightarrow D(k)$$

$$d_s(x) \leftrightarrow D_s(k)$$

$$s_\delta(x) \leftrightarrow S_\delta(k)$$

exist, then

$$D_s(k) = \int_{-\infty}^{+\infty} D(k')S_\delta(k - k')dk'. \quad (4.3)$$

The relation (4.3) follows from the convolution theorem of the Fourier transform. The spectrum of $d_s(x)$ is given by the convolution of the spectrum of the continuous-space function $d(x)$ with the the spectrum of the comb function. The form of $S_\delta(k)$ is, thus, important in determining the form of $D_s(k)$ and it is given by

$$S_\delta(k) = \int_{-\infty}^{+\infty} \left(\sum_{l=-\infty}^{l=+\infty} \delta(x - x_l) \right) e^{-i2\pi kx} dx = \sum_{l=-\infty}^{l=+\infty} e^{-i2\pi kx_l}.$$

¹The Fourier transform $D(k)$ of a function $d(x)$ is given by $D(k) = \int_{-\infty}^{+\infty} d(x)e^{-i2\pi kx} dx$.

It is now interesting to examine the special case when the sampling is done in a uniform fashion (i.e., on the nominal grid). Then $x_l = \bar{x}_l = l\Delta x$ for $l = -\infty, \dots, -1, 0, = 1, \dots, +\infty$. Substituting this in (4.1) we arrive at

$$S_\delta(k) = \sum_{l=-\infty}^{l=+\infty} e^{-i2\pi kl\Delta x} = \frac{1}{\Delta x} \sum_{l=-\infty}^{l=+\infty} \delta\left(k - \frac{l}{\Delta x}\right), \quad (4.4)$$

which is the Fourier transform of a Dirac comb with sampling interval Δx . Plugging (4.4) into (4.3) we get

$$\begin{aligned} D_s(k) &= \int_{-\infty}^{+\infty} D(k') \left[\frac{1}{\Delta x} \sum_{l=-\infty}^{l=+\infty} \delta\left(k - \frac{l}{\Delta x} - k'\right) \right] dk' \\ &= \sum_{l=-\infty}^{l=+\infty} \frac{1}{\Delta x} \int_{-\infty}^{+\infty} D(k') \delta\left(k - \frac{l}{\Delta x} - k'\right) dk' \\ &= \sum_{l=-\infty}^{l=+\infty} \frac{1}{\Delta x} D\left(k - \frac{l}{\Delta x}\right) \end{aligned}$$

We can see that the spectrum of the discrete space samples $d(l\Delta x)$ is a sum of periodic repetitions of the spectrum of $d(x)$. As is known from basic sampling theory, if the highest wavenumber of $D(k)$ is more than $\frac{1}{2\Delta x}$, then the shifted copies of $D(k)$ will partially overlap, a phenomenon known as aliasing.

In the more general case $x_l \neq \bar{x}_l$, the spectrum of the comb function is not a train of Dirac delta distributions. Examples of the spectrum of a nonuniform comb function are given in Fig. 4.1². A discussion over the form of these spectra can be found at the end of the next section.

Up to now we have examined the relation between the spectra of the continuous-space function $d(x)$ and its sampled version $d_s(x)$. We can now proceed with the effect of applying a low-pass filter to the sampled data. Let $h(x)$ denote a continuous-space function that acts as a low-pass filter. Then the spectrum of the filtered data is given by

$$D_F(k) = \int_{-\infty}^{+\infty} \int_{-\infty}^{+\infty} h(x') d_s(x - x') dx' e^{-i2\pi kx} dx = H(k) D_s(k), \quad (4.5)$$

which is given by the Fourier transform of the data convolved with the filter. $H(k)$ is the Fourier transform of $h(x)$ and the right hand side follows from the convolution theorem.

²The parameter α given under Fig. 4.1 controls the amount of permitted deviation that a receiver can have from its nominal position, as a percentage of Δx (see also Section 4.2).

Using (4.3) and (4.1) in (4.5) we get

$$D_{GF}(k) = H(k) \int_{-\infty}^{+\infty} D(k') \sum_{l=-\infty}^{l=+\infty} e^{-i2\pi(k-k')x_l} dk'. \quad (4.6)$$

Even if $H(k)$ is an ideal low-pass filter, the aliasing due to nonuniform sampling will be suppressed only in the stopband. The passband might still contain energy that has been present due to the convolution term. Due to this effect, disregarding the irregularities in sampling might not be a satisfactory solution for an anti-aliasing filter.

4.2 Stochastic sampling

Up to this point, the sampling points $x_l = \bar{x}_l + \delta x_l$ are assumed to be perfectly known. The effects of nonuniform sampling have been examined for a single realization of the input grid. It is useful to have a picture of the average effect of nonuniform sampling to the filtered spectrum of the recorded data. This can be done by assuming that the δx_l are random variables instead of fixed quantities. This means that $d(x)$ is sampled stochastically at a “jittered” location, close to the nominal sampling location (jittered sampling [5]). The receivers are laid out in the spatial interval $[0, X]$. We assume that the probability density function $p(\delta x_l)$ will be that of the uniform distribution over the interval $[-\frac{a\Delta x}{2}, \frac{a\Delta x}{2}]$:

$$p(\delta x_l) = \begin{cases} \frac{1}{a\Delta x}, & -\frac{a\Delta x}{2} \leq \delta x_l \leq \frac{a\Delta x}{2}, \quad 0 \leq a \leq 1 \\ 0 & \text{otherwise.} \end{cases} \quad (4.7)$$

This essentially means that the sampling location will have an equal probability to lie within a distance of $\frac{a\Delta x}{2}$ around the nominal sampling location.

The power spectral density (PSD) of $D_{GF}(k)$ reveals the influence of the irregularities in sampling. Since $h(x)$ is deterministic, the PSD of $D_{GF}(k)$ will be given by [9]

$$\lim_{X \rightarrow \infty} \frac{E \{ |D_{GF}(k)|^2 \}}{X} = |H(k)|^2 \lim_{X \rightarrow \infty} \frac{E \{ |D_s(k)|^2 \}}{X}. \quad (4.8)$$

The function is assumed $d(x)$ deterministic as well, therefore the PSD of $D_s(k)$ will be given by the convolution of $|D(k)|^2$ with the PSD of $S_\delta(k)$

$$\lim_{X \rightarrow \infty} \frac{E \{ |D_s(k)|^2 \}}{X} = \int_{-\infty}^{+\infty} |D(k')|^2 \lim_{X \rightarrow \infty} \frac{E \{ |S_\delta(k-k')|^2 \}}{X} dk'. \quad (4.9)$$

Dippé and Wold [5], building on the work of Beutler and Leneman [2], provide analytic expressions for the PSDs of various sampling functions. For the case of jittered sampling without missing samples the PSD becomes

$$\lim_{X \rightarrow \infty} \frac{E \{ |S_\delta(k)|^2 \}}{X} = \frac{1 - |\gamma(k)|^2}{\Delta x} + \frac{1}{\Delta x} |\gamma(k)|^2 \sum_{l=-\infty}^{+\infty} \delta(k - \frac{l}{\Delta x}) \quad (4.10)$$

where

$$\gamma(k) = \int_{-\infty}^{+\infty} p(\delta x_l) e^{-i2\pi k \delta x_l} d\delta x_l = \frac{\sin(\pi k a \Delta x)}{\pi k a \Delta x} = \text{sinc}(\pi k a \Delta x) \quad (4.11)$$

is the Fourier transform of the probability density function. Plugging (4.11) into (4.10) and moving $|\gamma(k)|^2$ in the summation we get

$$\lim_{X \rightarrow \infty} \frac{E \{|S_\delta(k)|^2\}}{X} = \frac{1 - \text{sinc}^2(\pi k a \Delta x)}{\Delta x} + \frac{1}{\Delta x} \sum_{l=-\infty}^{+\infty} \text{sinc}^2(\pi l a) \delta(k - \frac{l}{\Delta x}). \quad (4.12)$$

The behavior of the PSD of the sampling comb function for various values of a can be seen in Fig. 4.1. We see that,

- for $a = 0$, no jittering is allowed. All the geophones are placed at their nominal locations and the equation (4.12) becomes

$$\lim_{X \rightarrow \infty} \frac{E \{|S_\delta(k)|^2\}}{X} = \frac{1}{\Delta x} \sum_{l=-\infty}^{+\infty} \delta(k - \frac{l}{\Delta x}), \quad (4.13)$$

using $\text{sinc}(0) = 1$. As in (4.4), the result reduces to a uniform comb function in the wavenumber domain.

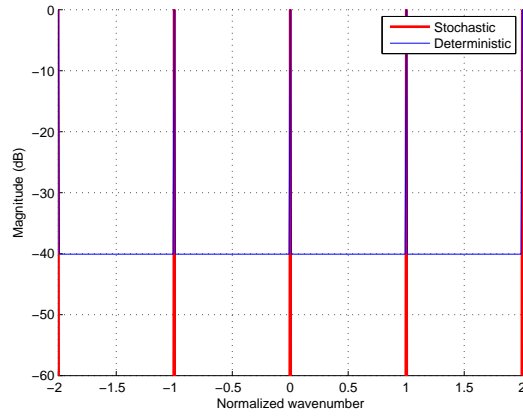
- for $a = 1$, δx_l is allowed to take values in the whole interval $[-\frac{\Delta x}{2}, \frac{\Delta x}{2}]$. Then (4.12) reduces to [5]

$$\lim_{X \rightarrow \infty} \frac{E \{|S_\delta(k)|^2\}}{X} = \frac{1 - \text{sinc}(\pi k \Delta x)}{\Delta x} + \frac{1}{\Delta x} \delta(k), \quad (4.14)$$

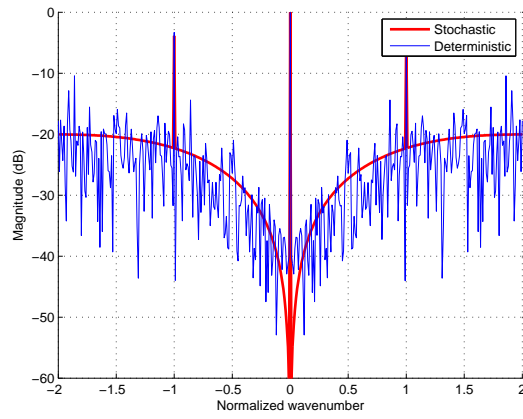
using that $\text{sinc}(l\pi) = 0$ for $l \neq 0$. It is noteworthy that when $a = 1$ there is but one impulse in the PSD. This means that the spectrum of $D_s(k)$ will no longer be a simple repetition of shifted copies of $D(k)$. This result suggests that by using randomized sampling it is possible to suppress impulsive aliasing. This possibility comes at the expense of introducing aliasing with more noise-like features, in our case represented by the first term [5].

- for $0 < a < 1$, an intermediate situation emerges. Multiple impulses are present, but each individual one is scaled by $\text{sinc}^2(\pi l a)$. Since the cardinal sine function is monotonically decreasing for $a \in [0, 1]$, it follows that all impulses except for the first one will have a smaller scale the closer a gets to 1. The opposite is true for the first term, which will generally decrease as a approaches 1.

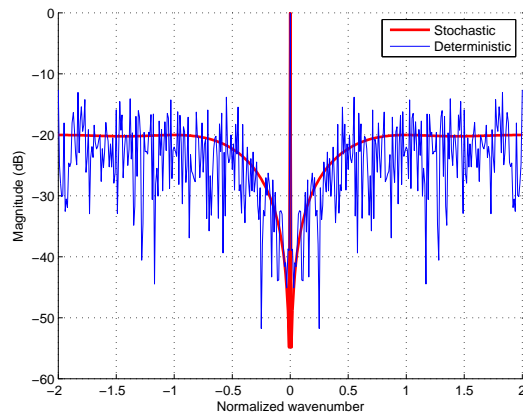
An example of the detrimental effects of nonuniform sampling can be seen in Fig. 4.2. On Fig. 4.2(a) can be seen spectrum of the uniformly sampled data. When the sampling pattern becomes nonuniform, spectral leakage occurs due to convolution with a nonimpulsive sampling pattern spectrum. The result is depicted in Fig. 4.1. As expected, simply applying a wavenumber filter to the nonuniformly sampled data will do very little about the spectral leakage in the stopband, a fact which can be clearly seen in Fig. 4.2(c).



(a) $a = 0$

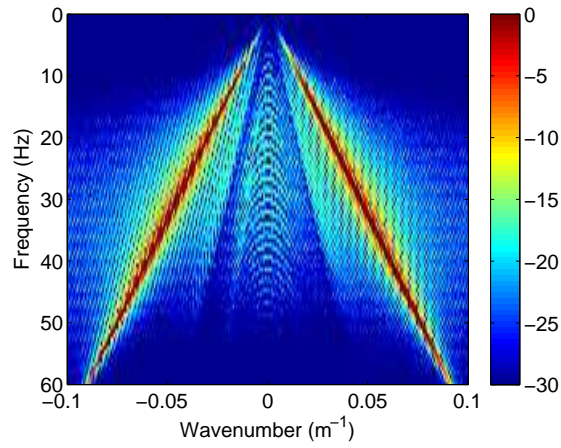


(b) $a = 0.5$

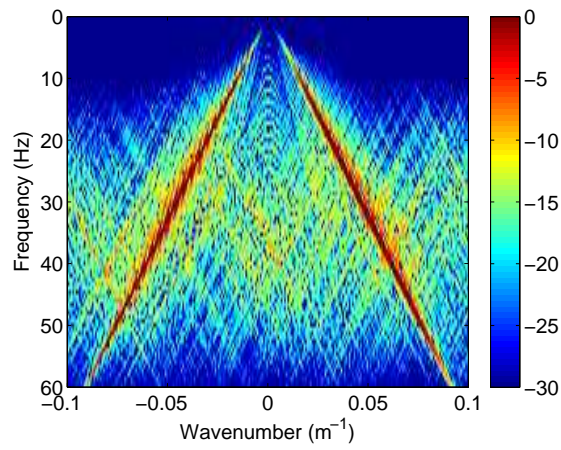


(c) $a = 1$

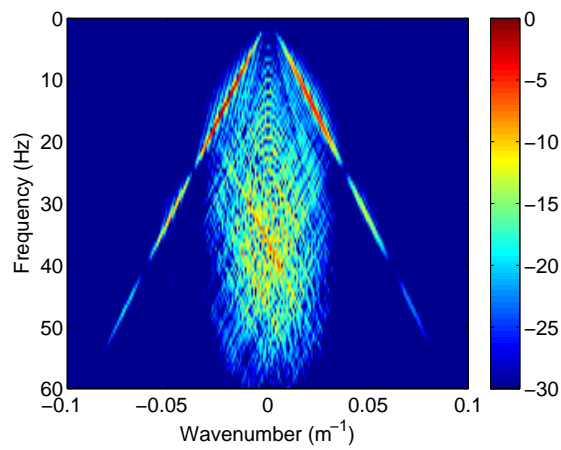
Figure 4.1: The spectrum of the comb function, as calculated for a single realization of the receiver locations (deterministic case) and the PSD of the stochastic case. The former is calculated using (4.1) and the latter using (4.12). Each plot is for a different value of a .



(a) Uniformly sampled data



(b) Nonuniformly sampled data



(c) Filtered nonuniformly sampled data

Figure 4.2: The effects of nonuniform sampling on the spectrum of the data ($\alpha = 0.8$).

Group forming for nonuniformly sampled data

5

5.1 The one-dimensional case

5.1.1 Spatial domain optimization

For this group forming method we will assume that the receiver locations are a subset of the dense grid nodes. This is not an overly restrictive requirement as the dense grid can be made to be dense enough so that the distance of the receiver from the closest dense grid node is within the accuracy of the location measurement. We also assume a FIR filter with L_f taps $h(\bar{x}_i)$ for $i = 0, 1, \dots, L_f - 1$ and that N_x receivers are dispersed in the interval $[0, N_x\Delta x)$. If the geophones were placed on the nominal grid, then the filtering step of group forming would be a simple discrete convolution with the filter

$$d_{\text{GF}}(\bar{x}_l) = \sum_{m=0}^{N_x-1} h(\bar{x}_{l-m})d(\bar{x}_m), \quad \text{for } l = L_f - 1, L_f, \dots, N_x - 1, \quad (5.1)$$

which can be compactly written as the matrix-vector product

$$\mathbf{d}_{\text{GF}} = \mathbf{H}\mathbf{d}_{\text{NOM}} \quad (5.2)$$

The vectors \mathbf{d}_{GF} and \mathbf{d}_{NOM} contain the filtered data and input data respectively, stacked as column vectors,

$$\mathbf{d}_{\text{GF}} = \begin{bmatrix} d_{\text{GF}}(\bar{x}_{L_f-1}) \\ d_{\text{GF}}(\bar{x}_{L_f}) \\ \vdots \\ d_{\text{GF}}(\bar{x}_{N_x-1}) \end{bmatrix}_{(N_x-L_f+1) \times 1}, \quad \mathbf{d}_{\text{NOM}} = \begin{bmatrix} d(\bar{x}_0) \\ d(\bar{x}_1) \\ \vdots \\ d(\bar{x}_{N_x-1}) \end{bmatrix}_{N_x \times 1}.$$

The matrix \mathbf{H} is actually a $(N_x - L_f + 1) \times N_x$ Toeplitz matrix with the first row constructed by padding the L_f filter coefficients with $N_x - L_f$ zeros. Thus the convolution is calculated only over the range $[(L_f - 1)\Delta x, (N_x - 1)\Delta x]$, where all samples entering the convolution are known. In this way the convolution edge effects are discarded. The structure of \mathbf{H} is given by:

$$\mathbf{H} = \begin{bmatrix} h(\bar{x}_{L_f-1}) & \cdots & h(\bar{x}_0) & \overbrace{0 \quad \cdots \quad 0}^{N_x-L_f} \\ 0 & h(\bar{x}_{L_f-1}) & \cdots & h(\bar{x}_0) & \ddots & \vdots \\ \vdots & \ddots & \ddots & \cdots & \ddots & 0 \\ 0 & \cdots & 0 & h(\bar{x}_{L_f-1}) & \cdots & h(\bar{x}_0) \end{bmatrix}_{(N_x-L_f+1) \times N_x} \quad (5.3)$$

A different scheme has to be devised when the input locations do not coincide with the nominal grid. Since only the values $d(\bar{x}_i + \delta x_i)$ are known, a reasonable requirement would be to find a set of filters $g_l(\bar{x}_n)$ such that

$$d_{\text{GF}}(\bar{x}_l) = \sum_{m=0}^{N_x-1} h(\bar{x}_l - \bar{x}_m) d(\bar{x}_m) = \sum_{n=0}^{N_x M_x - 1} g_l(\bar{x}_l - \bar{x}_n) s(\bar{x}_n) d(\bar{x}_n), \quad (5.4)$$

for $l = L_f - 1, L_f, \dots, N_x - 1$. In matrix notation (5.4) becomes

$$\mathbf{H} \mathbf{d}_{\text{NOM}} = \mathbf{G} \mathbf{S} \mathbf{d}_{\text{DEN}} \quad (5.5)$$

where

$$\mathbf{S} = \text{diag} \left(\begin{bmatrix} s(\bar{x}_0) \\ s(\bar{x}_1) \\ \vdots \\ s(\bar{x}_{N_x M_x - 1}) \end{bmatrix} \right)_{N_x M_x \times N_x M_x} \quad \text{and} \quad \mathbf{d}_{\text{DEN}} = \begin{bmatrix} d(\bar{x}_0) \\ d(\bar{x}_1) \\ \vdots \\ d(\bar{x}_{N_x M_x - 1}) \end{bmatrix}_{N_x M_x \times 1}. \quad (5.6)$$

Each element $(l - L_f + 1, n)$ of the $(N_x - L_f + 1) \times N_x M_x$ matrix \mathbf{G} is equal to $g_l(\bar{x}_n)$. We require that $g_l(\bar{x}_n) = 0$ for $n - (l - L_f + 1)M_x \geq L_f M_x$. Then, each row of \mathbf{G} represents a filter with the same spatial support as that of each row of \mathbf{H} . Unlike \mathbf{H} though, each row of \mathbf{G} is not necessarily a shifted version of the first row. Therefore it can be said that \mathbf{G} represents a linear space-*varying* (LSV) filter in contrast to \mathbf{H} which represents a linear space invariant (LSI) filter. Also note that the output of \mathbf{G} is defined on the nominal grid.

The relation (5.6) still depends on samples of the wavefield collected on the nominal grid, which are not available in reality. In order to drop the dependence on \mathbf{d}_{NOM} , a relation between \mathbf{d}_{DEN} and \mathbf{d}_{NOM} must be established. If $d(x)$ is bandlimited in the wavenumber domain, an approximate relation exists between the values of the wavefield on the nominal grid $d(\bar{x}_q)$ and the values on the dense grid $d(\bar{x}_n)$:

$$d(\bar{x}_n) \approx \sum_{q=0}^{N_x-1} \text{sincd}(N_x; \bar{x}_n, \bar{x}_q) d(\bar{x}_q) \quad (5.7)$$

This is a discretized version of the well-known sinc interpolation. The function $\text{sincd}(\cdot)$ is defined to be

$$\text{sincd}(N_x; \bar{x}_n, \bar{x}_q) = \begin{cases} \frac{\sin\left(\frac{\pi}{\Delta x}(\bar{x}_n - \bar{x}_q)\right)}{N_x \sin\left(\frac{\pi}{N_x \Delta x}(\bar{x}_n - \bar{x}_q)\right)} & \text{if } N_x \text{ odd and } \bar{x}_n \neq \bar{x}_q, \\ \frac{\sin\left(\frac{(N_x-1)\pi}{N_x \Delta x}(\bar{x}_n - \bar{x}_q)\right)}{N_x \sin\left(\frac{\pi}{N_x \Delta x}(\bar{x}_n - \bar{x}_q)\right)} + \frac{1}{N_x} \cos\left(\frac{\pi}{\Delta x}(\bar{x}_n - \bar{x}_q)\right) & \text{if } N_x \text{ even and } \bar{x}_n \neq \bar{x}_q \\ 1 & \text{if } \bar{x}_n = \bar{x}_q. \end{cases} \quad (5.8)$$

The equation (5.7) can be written as a matrix-vector product

$$\mathbf{d}_{\text{DEN}} \approx \mathbf{Q} \mathbf{d}_{\text{NOM}} \quad (5.9)$$

where

$$\mathbf{Q} = \begin{bmatrix} \text{sincd}(N_x; \bar{x}_0, \bar{x}_0) & \cdots & \text{sincd}(N_x; \bar{x}_0, \bar{x}_{N_x-1}) \\ \vdots & & \vdots \\ \text{sincd}(N_x; \bar{x}_{N_x M_x - 1}, \bar{x}_0) & \cdots & \text{sincd}(N_x; \bar{x}_{N_x M_x - 1}, \bar{x}_{N_x - 1}) \end{bmatrix}_{N_x M_x \times N_x}$$

Plugging (5.9) into (5.6) we get

$$\mathbf{H} \mathbf{d}_{\text{NOM}} \approx \mathbf{G} \mathbf{S} \mathbf{Q} \mathbf{d}_{\text{NOM}}, \quad (5.10)$$

which should hold for every possible \mathbf{d}_{NOM} . A way to accomplish this is to find a matrix \mathbf{G} such that

$$\mathbf{H} \approx \mathbf{G} \mathbf{S} \mathbf{Q}. \quad (5.11)$$

A way to find such a matrix \mathbf{G} is to solve the least squares problem

$$\min_{\mathbf{G}} \{ \|\mathbf{H} - \mathbf{G} \mathbf{S} \mathbf{Q}\|_F^2 \}. \quad (5.12)$$

From its definition it follows that the Frobenius norm can be written as a sum of the ℓ_2 norms of its rows:

$$\|\mathbf{H} - \mathbf{G} \mathbf{S} \mathbf{Q}\|_F^2 = \sum_{l=0}^{N_x - L_f} \|\text{row}(\mathbf{H}; l) - \text{row}(\mathbf{G}; l) \mathbf{S} \mathbf{Q}\|_2^2. \quad (5.13)$$

Each row of \mathbf{G} contains elements that should not be optimized. These are the elements n for which $n - (l - L_f + 1)M_x \geq L_f M_x$. This ensures that each row of \mathbf{G} is a FIR filter with the same spatial support as $h(x)$. The elements of each row of \mathbf{G} that are to be excluded from optimization can be removed together with the corresponding rows of \mathbf{S} . Let \mathbf{S}_l be the submatrix of \mathbf{S} formed by removing the rows that correspond to variables of $\text{row}(\mathbf{G}; l) = \mathbf{g}_l$ that should not be optimized. Then

$$\|\mathbf{H} - \mathbf{G} \mathbf{S} \mathbf{Q}\|_F^2 = \sum_{l=0}^{N_x - L_f} \|\text{row}(\mathbf{H}; l) - \mathbf{g}_l^T \mathbf{S}_l \mathbf{Q}\|_2^2 \quad (5.14)$$

Since (5.14) is a summation of nonnegative quantities, solving (5.12) is the same as solving

$$\min_{\mathbf{g}_l} \{ \|\text{row}(\mathbf{H}; l) - \mathbf{g}_l^T \mathbf{S}_l \mathbf{Q}\|_2^2 \} \text{ for } l = 0, 1, \dots, N_x - 1. \quad (5.15)$$

\mathbf{S}_l can be eliminated since its effect is to set certain elements of \mathbf{g}_l and rows of \mathbf{Q} to zero. Let $\tilde{\mathbf{g}}_l$ be \mathbf{g}_l after removal of those elements which would have been set to zero by the product $\mathbf{g}_l^T \mathbf{S}_l$. Similarly let $\tilde{\mathbf{Q}}_l$ be a reduced version of \mathbf{Q} that only retains those rows that would not be set to zero by the product $\mathbf{S}_l \mathbf{Q}$. Then (5.15) becomes

$$\min_{\tilde{\mathbf{g}}_l} \{ \|\text{row}(\mathbf{H}; l) - \tilde{\mathbf{g}}_l^T \tilde{\mathbf{Q}}_l\|_2^2 \} \text{ for } l = 0, 1, \dots, N_x - 1. \quad (5.16)$$

The closed form solution is given by

$$\tilde{\mathbf{g}}_l = (\tilde{\mathbf{Q}}_l^T)^\dagger \text{row}(\mathbf{H}; l)^T. \quad (5.17)$$

5.1.2 Wavenumber domain optimization

Instead of the linear convolution operator defined in (5.2), the circular convolution operator could be used to perform the filtering.

$$d'_{\text{GF}}(\bar{x}_l) = \sum_{m=0}^{N_x-1} h(\bar{x}_{(l-m) \bmod N_x}) d(\bar{x}_m), \quad \text{for } l = 0, 1, \dots, N_x - 1. \quad (5.18)$$

The objective is to find a set of filters $g'_l(\bar{x}_n)$ such that

$$d'_{\text{GF}}(\bar{x}_l) = \sum_{n=0}^{N_x M_x} g'_l(\bar{x}_{lM_x - n \bmod (N_x M_x)}) d(\bar{x}_n) \quad \text{for } l = 0, 1, \dots, N_x - 1.$$

Just as with $g_l(\bar{x}_n)$, each $g'_l(\bar{x}_n)$ should have a bounded support, which now takes the form

$$g'_l(\bar{x}_n) = 0 \quad \text{if } (lM_x - n) \bmod (N_x M_x) \geq L_f M_x. \quad (5.19)$$

We can now start exploring a new method for creating a LSV filter, denoted by the $N_x \times N_x M_x$ matrix \mathbf{G}' whose element (l, n) is $g'_l(\bar{x}_n)$. We begin by defining

$$\mathbf{h}_{\text{PAD}} = [h(\bar{x}_0), h(\bar{x}_1), \dots, h(\bar{x}_{L_f-1}), \overbrace{0, \dots, 0}^{N_x - L_f}]^T. \quad (5.20)$$

The circular convolution can be then written in matrix notation as

$$\mathbf{d}'_{\text{GF}} = \mathbf{H}' \mathbf{d}_{\text{NOM}} = \text{circ}(\mathbf{h}_{\text{PAD}}) \mathbf{d}_{\text{NOM}}. \quad (5.21)$$

where \mathbf{d}'_{GF} is a vector of the stacked values $d'_{\text{GF}}(t, \bar{x}_l)$ for $l = 0, 1, \dots, N_x - 1$.

Let \mathbf{F} be a $N_x \times N_x$ discrete Fourier transform (DFT) matrix such that $\frac{1}{N_x} \mathbf{F}^H \mathbf{F} = \mathbf{I}$. The spectra of \mathbf{d}'_{GF} and \mathbf{d}_{NOM} have a simple relation that is given by the DFT transform:

$$\mathbf{F} \mathbf{d}'_{\text{GF}} = \mathbf{F} \mathbf{H}' \mathbf{d}_{\text{NOM}} = \frac{1}{N_x} (\mathbf{F} \mathbf{H}' \mathbf{F}^H) (\mathbf{F} \mathbf{d}_{\text{NOM}}) \quad (5.22)$$

From the fact that the columns of DFT matrices form the eigenvectors of circulant matrices, it follows that DFT matrices can diagonalize circulant matrices [4]. Therefore, \mathbf{H}' can be factorized as

$$\mathbf{H}' = \frac{1}{N_x} \mathbf{F}^H \text{diag}(\mathbf{F} \mathbf{h}_{\text{PAD}}) \mathbf{F} \quad (5.23)$$

Note that the relation above holds for circulant matrices. Unlike the spatial domain formulation of the problem, the first $L_f - 1$ rows of \mathbf{H}' that produce the edge values $d'_{\text{GF}}(t, \bar{x}_l)$, $l = 0, 1, \dots, L_f - 2$ have to be present, to make \mathbf{H}' circulant. Plugging (5.23) into (5.22) yields

$$\mathbf{F} \mathbf{d}'_{\text{GF}} = \text{diag}(\mathbf{F} \mathbf{h}_{\text{PAD}}) (\mathbf{F} \mathbf{d}_{\text{NOM}}) \quad (5.24)$$

It can be seen from (5.24) that each wavenumber component of \mathbf{d}'_{GF} is simply a scaled and phase shifted version of the corresponding wavenumber component in \mathbf{d}_{NOM} . This is the expected behavior of a LSI FIR filter. Since we want \mathbf{d}'_{GF} to be a low-pass

filtered version of \mathbf{d}_{NOM} , it is reasonable to express this requirement in the wavenumber domain:

$$\frac{1}{N_x} \mathbf{F} \mathbf{H}' \mathbf{F}^H (\mathbf{F} \mathbf{d}_{\text{NOM}}) \approx \frac{1}{N_x} \mathbf{F} \mathbf{G}' \mathbf{S} \mathbf{Q} \mathbf{F}^H (\mathbf{F} \mathbf{d}_{\text{NOM}}), \quad (5.25)$$

which should hold for every $\mathbf{F} \mathbf{d}_{\text{NOM}}$. Therefore

$$\mathbf{F} \mathbf{H}' \mathbf{F}^H \approx \mathbf{F} \mathbf{G}' \mathbf{S} \mathbf{Q} \mathbf{F}^H, \quad (5.26)$$

When the output grid is on the nominal grid, the indexes of the variables in \mathbf{G}' that should *not* be optimized are the indexes of the zero elements of

$$\text{circ}([\mathbf{1}_{L_f}^T \ \mathbf{0}_{N_x-L_f}^T]) \otimes \mathbf{1}_{M_x}^T, \quad (5.27)$$

where $\mathbf{1}_{L_f}$ is a column vector of L_f ones and $\mathbf{0}_{N_x-L_f}$ a column vector of zeros. This formulation follows from (5.19). Not optimizing with respect to the variables corresponding the zeros of (5.27) ensures that the filter outputs of \mathbf{G}' are at the same locations as those of \mathbf{H}' and that the each filter in \mathbf{G}' has the same physical length as each filter in \mathbf{H}' .

The filter $h(\bar{x}_i)$ which we try to approximate in (5.26) is itself an approximation of the ideal low-pass filter. Using the wavenumber domain formulation it is possible to replace $\mathbf{F} \mathbf{H}' \mathbf{F}^H$ with an ideal low-pass filter. Let

$$H_w(k) = \begin{cases} 1, & \text{if } k \in [-k_{pass}, +k_{pass}] \\ 0, & \text{otherwise} \end{cases} \quad (5.28)$$

be the ideal low-pass wavenumber response with bandwidth $2k_{pass}$. The sampled and diagonalized ideal wavenumber response can be then constructed by sampling $H_w(k)$:

$$\mathbf{H}_w = \text{diag} \left(\begin{bmatrix} H_w(b + 0 \frac{2\pi}{N_x}) \\ H_w(b + 1 \frac{2\pi}{N_x}) \\ \vdots \\ H_w(b + (N_x - 1) \frac{2\pi}{N_x}) \end{bmatrix} \right) \quad (5.29)$$

where $b = (-1 + 1/N_x)\pi$ when N_x is odd and $b = -\pi$ when N_x is even. It is possible then to replace $\mathbf{F} \mathbf{H}' \mathbf{F}^H$ in (5.26) with \mathbf{H}_w . The optimization problem thus now becomes

$$\min_{\mathbf{G}'} \left\{ \|\mathbf{W} \odot (\mathbf{H}_w - \frac{1}{N_x} \mathbf{F} \mathbf{G}' \mathbf{S} \mathbf{Q} \mathbf{F}^H)\|_F^2 \right\}. \quad (5.30)$$

The matrix \mathbf{W} applies weights that can be different for the diagonal elements and the offdiagonal elements. In this way we may attempt to control the tradeoff between accurate approximation of the low-pass filter and the amount of spectral leakage.

The expression can be simplified by eliminating \mathbf{S} from the product $\mathbf{G}' \mathbf{S} \mathbf{Q}$. Let $\tilde{\mathbf{G}}'$ be a matrix formed by the columns of \mathbf{G}' that have indexes corresponding to the nonzero elements of \mathbf{S} . Similarly, let $\tilde{\mathbf{Q}}$ be a matrix formed by keeping those rows of \mathbf{Q} that correspond to the nonzero elements of \mathbf{S} . Then (5.30) can be written as

$$\min_{\mathbf{G}'} \left\{ \|\mathbf{W} \odot (\mathbf{H}_w - \frac{1}{N_x} \mathbf{F} \tilde{\mathbf{G}}' \tilde{\mathbf{Q}} \mathbf{F}^H)\|_F^2 \right\} \quad (5.31)$$

It is possible to convert the Frobenius norm in (5.31) to an ℓ_2 norm by vectorizing the problem. It is then easy to optimize only over the variables in \mathbf{G}' and discard the zeros. Using the identity $\text{vec}(\mathbf{ABC}) = (\mathbf{C}^T \otimes \mathbf{A}) \text{vec}(\mathbf{B})$, (5.31) becomes

$$\min_{\text{vec}(\mathbf{G}')} \left\{ \left\| \text{vec}(\mathbf{W} \odot \mathbf{H}_w) - \text{diag}(\text{vec}(\mathbf{W})) (\mathbf{F}^* \tilde{\mathbf{Q}}^T \otimes \frac{1}{N_x} \mathbf{F}) \text{vec}(\tilde{\mathbf{G}}') \right\|_2^2 \right\}, \quad (5.32)$$

where the asterisk denotes the complex conjugate. Let

$$\begin{aligned} \tilde{\mathbf{U}} &= \text{diag}(\text{vec}(\mathbf{W})) (\mathbf{F}^* \tilde{\mathbf{Q}}^T \otimes \frac{1}{N_x} \mathbf{F}) \\ \tilde{\mathbf{g}}' &= \text{vec}(\tilde{\mathbf{G}}'). \end{aligned}$$

The elements of $\tilde{\mathbf{g}}'$ and rows of $\tilde{\mathbf{U}}$ that should be removed due to the limited spatial support of the filter $g'_i(\bar{x}_n)$ are given by the indexes of those elements of $\tilde{\mathbf{g}}'$ that correspond to the zero elements of $g'_i(\bar{x}_n)$. If we call $\tilde{\tilde{\mathbf{g}}}'$ and $\tilde{\tilde{\mathbf{U}}}$ the results after the corresponding row and element removal, the solution is given by

$$\tilde{\tilde{\mathbf{g}}}' = \tilde{\tilde{\mathbf{U}}}^\dagger \text{diag}(\text{vec}(\mathbf{W})) \text{vec}(\mathbf{H}_w)$$

\mathbf{G}' can be reconstructed from the elements of $\tilde{\tilde{\mathbf{g}}}'$ and can be applied to the nonuniformly sampled data.

5.2 The two-dimensional case

5.2.1 Spatial domain optimization

As in the one-dimensional case, we will assume that the receiver locations are a subset of the dense grid nodes. The FIR filter will be two-dimensional with $L_{fx} \times L_{fy}$ taps, $h(\bar{x}_i, \bar{y}_j)$ for $i = 0, 1, \dots, L_{fx} - 1$ and $j = 0, 1, \dots, L_{fy} - 1$ that $N_x \times N_y$ receivers are dispersed on the plane $[0, N_x \Delta x) \times [0, N_y \Delta y)$. If the geophones were placed on the nominal grid, filtering the gathered data would amount to a 2D convolution

$$d_{\text{GF}}(\bar{x}_i, \bar{y}_j) = \sum_{m=0}^{N_x-1} \sum_{n=0}^{N_y-1} h(\bar{x}_{i-m}, \bar{y}_{j-n}) d(\bar{x}_m, \bar{y}_n). \quad (5.33)$$

Note that we do not make any assumption about the separability of the filter. The equation (5.33) is analogous to (5.1) and holds both for separable and non-separable filters. In order to convert (5.33) into matrix notation, a convention should be used on how should the values of $d(x, y)$ should be stacked in a vector. Unless otherwise mentioned, we will assume that data is stacked by varying x in $d(x, y)$ keeping y constant,

i.e.

$$\mathbf{d}_{\text{GF}} = \begin{bmatrix} d(\bar{x}_{L_{fx}-1}, \bar{y}_{L_{fy}-1}) \\ d(\bar{x}_{L_{fx}}, \bar{y}_{L_{fy}-1}) \\ \vdots \\ d(\bar{x}_{N_x-1}, \bar{y}_{L_{fy}-1}) \\ \vdots \\ d(\bar{x}_{N_x-1}, \bar{y}_{N_y-1}) \end{bmatrix}_{\substack{(N_x-L_{fx}+1) \cdot \\ (N_y-L_{fy}+1) \times 1}} \quad \mathbf{d}_{\text{NOM}} = \begin{bmatrix} d(\bar{x}_0, \bar{y}_0) \\ d(\bar{x}_1, \bar{y}_0) \\ \vdots \\ d(\bar{x}_{N_x-1}, \bar{y}_0) \\ \vdots \\ d(\bar{x}_{N_x-1}, \bar{y}_{N_y-1}) \end{bmatrix}_{N_x N_y \times 1} \quad (5.34)$$

It is now possible to construct a matrix \mathcal{H} that can perform the convolution operation in (5.33) as a matrix multiplication for data stacked in such a way. This matrix is a block matrix that has the Toeplitz-like structure seen in (5.3) at a block level. Each individual block also has this structure within itself. Let \mathbf{H}_l be a matrix block of \mathcal{H} . Then

$$\mathbf{H}_l = \begin{bmatrix} h(\bar{x}_{L_{fx}-1}, \bar{y}_l) & \cdots & h(\bar{x}_0, \bar{y}_l) & \cdots & 0 \\ 0 & h(\bar{x}_{L_{fx}-1}, \bar{y}_l) & \cdots & h(\bar{x}_0, \bar{y}_l) & \vdots \\ \vdots & \ddots & \ddots & \ddots & 0 \\ 0 & \cdots & h(\bar{x}_{L_{fx}-1}, \bar{y}_l) & \cdots & h(\bar{x}_0, \bar{y}_l) \end{bmatrix}_{(N_x-L_{fx}+1) \times N_x} \quad (5.35)$$

and \mathcal{H} can be constructed using \mathbf{H}_l as building blocks:

$$\mathcal{H} = \begin{bmatrix} \mathbf{H}_{L_{fy}-1} & \mathbf{H}_{L_{fy}-2} & \cdots & \mathbf{H}_0 & \mathbf{0} & \cdots & \mathbf{0} \\ \mathbf{0} & \mathbf{H}_{L_{fy}-1} & \mathbf{H}_{L_{fy}-2} & \cdots & \mathbf{H}_0 & \cdots & \vdots \\ \vdots & \ddots & \ddots & \ddots & \ddots & \ddots & \mathbf{0} \\ \mathbf{0} & \cdots & \mathbf{0} & \mathbf{H}_{L_{fy}-1} & \mathbf{H}_{L_{fy}-2} & \cdots & \mathbf{H}_0 \end{bmatrix}_{\substack{(N_x-L_{fx}+1)(N_y-L_{fy}+1) \\ \times N_x N_y}} \quad (5.36)$$

The filtering can next be performed by the matrix multiplication

$$\mathbf{d}_{\text{GF}} = \mathcal{H} \mathbf{d}_{\text{NOM}}. \quad (5.37)$$

In a similar manner to the one-dimensional case, the objective is to calculate the coefficients of a two dimensional LSV filter $g_{i,j}(\bar{x}_m, \bar{y}_n)$ that should ideally give the same output values $d_{\text{GF}}(\bar{x}_i, \bar{y}_j)$ when applied to the nonuniformly sampled data:

$$d_{\text{GF}}(\bar{x}_i, \bar{y}_j) = \sum_{m=0}^{N_x M_x - 1} \sum_{n=0}^{N_y M_y - 1} g_{i,j}(\bar{x}_i - \bar{x}_m, \bar{y}_j - \bar{y}_n) s(\bar{x}_m, \bar{y}_n) d(\bar{x}_m, \bar{y}_n)$$

or in matrix notation

$$\mathbf{d}_{\text{GF}} = \mathcal{G} \mathbf{S} \mathbf{d}_{\text{DEN}} \quad (5.38)$$

where \mathcal{S} is

$$\mathcal{S} = \text{diag} \left(\begin{bmatrix} s(\bar{x}_0, \bar{y}_0) \\ s(\bar{x}_1, \bar{y}_0) \\ \vdots \\ s(\bar{x}_{N_x M_x - 1}, \bar{y}_0) \\ \vdots \\ s(\bar{x}_{N_x M_x - 1}, \bar{y}_{N_y M_y - 1}) \end{bmatrix} \right) \quad \text{and} \quad \mathbf{d}_{\text{DEN}} = \begin{bmatrix} d(\bar{x}_0, \bar{y}_0) \\ d(\bar{x}_1, \bar{y}_0) \\ \vdots \\ d(\bar{x}_{N_x M_x - 1}, \bar{y}_0) \\ \vdots \\ d(\bar{x}_{N_x M_x - 1}, \bar{y}_{N_y M_y - 1}) \end{bmatrix}. \quad (5.39)$$

The matrix \mathcal{S} has size $N_x M_x N_y M_y \times N_x M_x N_y M_y$ and the vector \mathbf{d}_{NOM} now has size $N_x N_y \times 1$. \mathcal{G} is constructed in a similar manner as \mathcal{H} , except that the filter now has $N_x M_x \times N_y M_y$ taps and is not required to be the same for each output location.

In the 2D extension the interpolation kernel first interpolates along the x -axis and then interpolates the result along the y -axis:

$$d(\bar{x}_m, \bar{y}_n) \approx \sum_{i=0}^{N_x-1} \sum_{j=0}^{N_y-1} \text{sincd}(N_x; \bar{x}_i, \bar{x}_m) \text{sincd}(N_y; \bar{y}_j, \bar{y}_n) d(\bar{x}_i, \bar{y}_j).$$

With the aid of the Kronecker product this can be written as

$$\mathbf{d}_{\text{DEN}} \approx (\mathbf{Q}_y \otimes \mathbf{Q}_x) \mathbf{d}_{\text{NOM}} \quad (5.40)$$

where \mathbf{Q}_x and \mathbf{Q}_y have dimensions $N_x M_x \times N_x$ and $N_y M_y \times N_y$ respectively and are defined in a similar fashion as \mathbf{Q} . Plugging (5.40) into (5.38) we get

$$\mathcal{H} \mathbf{d}_{\text{NOM}} \approx \mathcal{G} \mathcal{S} (\mathbf{Q}_x \otimes \mathbf{Q}_y) \mathbf{d}_{\text{NOM}} \quad (5.41)$$

which we would like to hold for every \mathbf{d}_{NOM} . As in the one-dimensional case, we can optimize

$$\min_{\mathcal{G}} \{ \|\mathcal{H} - \mathcal{G} \mathcal{S} (\mathbf{Q}_x \otimes \mathbf{Q}_y)\|_F^2 \} \quad (5.42)$$

per row of \mathcal{G} .

5.2.2 Wavenumber domain optimization

It is also possible to extend the wavenumber domain optimization to the two-dimensional case. In a manner analogous to the one-dimensional case, the spatial domain formulation can be restated as

$$(\mathbf{F}_y \otimes \mathbf{F}_x) \mathcal{H}' (\mathbf{F}_y \otimes \mathbf{F}_x)^H = (\mathbf{F}_y \otimes \mathbf{F}_x) \mathcal{G}' \mathcal{S} (\mathbf{Q}_y \otimes \mathbf{Q}_x) (\mathbf{F}_y \otimes \mathbf{F}_x)^H \quad (5.43)$$

were \mathbf{F}_x and \mathbf{F}_y are $N_x \times N_x$ and $N_y \times N_y$ DFT matrices respectively. The matrix \mathcal{H}' has block circulant - circulant block structure,

$$\mathcal{H}' = \begin{bmatrix} \mathbf{H}'_0 & \mathbf{0} & \cdots & \mathbf{0} & \mathbf{H}'_{L_{fy}-1} & \cdots & \mathbf{H}'_1 \\ \mathbf{H}'_1 & \mathbf{H}'_0 & \ddots & \ddots & \ddots & \ddots & \vdots \\ \vdots & \mathbf{H}'_1 & \ddots & \ddots & \ddots & \ddots & \mathbf{H}'_{L_{fy}-1} \\ \mathbf{H}'_{L_{fy}-1} & \vdots & \ddots & \mathbf{H}'_0 & \ddots & \ddots & \mathbf{0} \\ \mathbf{0} & \mathbf{H}'_{L_{fy}-1} & \ddots & \mathbf{H}'_1 & \mathbf{H}'_0 & \ddots & \vdots \\ \vdots & \ddots & \ddots & \vdots & \mathbf{H}'_1 & \ddots & \mathbf{0} \\ \mathbf{0} & \cdots & \mathbf{0} & \mathbf{H}'_{L_{fy}-1} & \vdots & \ddots & \mathbf{H}'_0 \end{bmatrix}_{N_x N_y \times N_x N_y}. \quad (5.44)$$

Each block-row has $N_y - L_{fy}$ blocks of zeros, so that each block-row contains N_y blocks. Each block \mathbf{H}'_l is a circulant matrix given by

$$\mathbf{H}'_l = \text{circ}([h(\bar{x}_0, \bar{y}_l), h(\bar{x}_1, \bar{y}_l), \cdots, h(\bar{x}_{N_x-1}, \bar{y}_l), \overbrace{0 \cdots 0}^{N_x - L_{fx}}]). \quad (5.45)$$

The matrix \mathcal{H}' differs from \mathcal{H} in that $\mathcal{H}'\mathbf{d}_{\text{NOM}}$ also includes circular convolution edge effects in the output. In this form however, \mathcal{H}' can be diagonalized by $\mathbf{F}_y \otimes \mathbf{F}_x$ [4]. We can therefore replace the product $(\mathbf{F}_y \otimes \mathbf{F}_x)\mathcal{H}'(\mathbf{F}_y \otimes \mathbf{F}_x)^H$ with an ideal low-pass filter. If the ideal low-pass filter is circularly symmetric, then its wavenumber response will be given by

$$\mathcal{H}_w(k_x, k_y) = \begin{cases} 1, & \text{if } \sqrt{k_x^2 + k_y^2} \in [-k_{pass}, k_{pass}] \\ 0, & \text{otherwise.} \end{cases} \quad (5.46)$$

where k_{pass} denotes the end of the bandpass region of the filter. A diagonal matrix \mathcal{H}_w can be constructed representing the ideal low-pass filter in a diagonalized form. This diagonalized form can be constructed by sampling $\mathcal{H}_w(k_x, k_y)$ and stacking the samples along the diagonal of \mathcal{H}_w

$$\mathcal{H}_w = \text{diag} \left(\begin{bmatrix} \mathcal{H}_w(b_x + 0\frac{2\pi}{N_x}, b_y + 0\frac{2\pi}{N_y}) \\ \vdots \\ \mathcal{H}_w(b_x + (N_x - 1)\frac{2\pi}{N_x}, b_y + 0\frac{2\pi}{N_y}) \\ \mathcal{H}_w(b_x + 0\frac{2\pi}{N_x}, b_y + 1\frac{2\pi}{N_y}) \\ \vdots \\ \mathcal{H}_w(b_x + (N_x - 1)\frac{2\pi}{N_x}, b_y + (N_y - 1)\frac{2\pi}{N_y}) \end{bmatrix} \right). \quad (5.47)$$

The constants b_x and b_y depend on whether N_x and N_y are even or odd integers. When N_x is odd, $b_x = (-1 + 1/N_x)\pi$. When N_x is even, $b_x = -\pi$. The value of b_y is calculated in a similar way. This has the effect of sampling $\mathcal{H}_w(k_x, k_y)$ in $[-\pi, +\pi]$ in both dimensions.

It is then possible to optimize

$$\min_{\mathcal{G}'} \left\{ \left\| \mathbf{W} \odot (\mathcal{H}_w - (\mathbf{F}_y \otimes \mathbf{F}_x) \mathcal{G}' \mathcal{S} (\mathbf{Q}_y \otimes \mathbf{Q}_x) (\mathbf{F}_y \otimes \mathbf{F}_x)^H) \right\|_F^2 \right\}, \quad (5.48)$$

in the same manner as (5.31). The variables in \mathcal{G}' not to be optimized when the output locations lie on the nominal grid are given by the indexes of the zeros in

$$\left(\text{circ}([\mathbf{1}_{L_{fy}}^T, \mathbf{0}_{N_y - L_{fy}}^T]) \otimes \mathbf{1}_{M_y}^T \right) \otimes \left(\text{circ}([\mathbf{1}_{L_{fx}}^T, \mathbf{0}_{N_x - L_{fx}}^T]) \otimes \mathbf{1}_{M_x}^T \right).$$

5.3 Geometry compensating digital group forming

An alternative way of calculating coefficients for filtering irregularly sampled data is presented in [8]. We implemented their method and used it for the purpose of benchmarking the performance of the algorithms described in the previous section. In this section an outline of their method will be presented, as well as a 1D adaptation. This is done in order to examine more closely the differences and similarities with the methods previously discussed.

5.3.1 The two-dimensional case

We begin with the 2D case since this is the case that is discussed in [8]. Recall from (5.33) that

$$d_{\text{GF}}(x, y) = \sum_{i=0}^{L_{fx}-1} \sum_{j=0}^{L_{fy}-1} h(x - \bar{x}_i, y - \bar{y}_j) d(\bar{x}_i, \bar{y}_j), \quad (5.49)$$

Let $h_c(x, y)$ and $d_c(x, y)$ be continuous and smooth functions for which $h_c(x, y) = h(x, y)$ and $d_c(x, y) = d(x, y)$ holds, when $x = i\Delta x$, $i = 0, 1, \dots, L_{fx}$ and $j = 0, 1, \dots, L_{fy}$, $j = 0, 1, \dots, L_{fy}$. The functions $h_c(x, y)$ and $d_c(x, y)$ can be considered as continuous interpolations approximating $h(x, y)$ and $d(x, y)$ respectively and have zero error at the nominal grid points. 2D cubic interpolation is used in [8], but also other interpolation methods are suggested, such as spline, sinc and polynomials.

Within the accuracy of the trapezoidal rule, (5.49) can be approximated as

$$d_{\text{GF}}(x, y) \approx \frac{1}{\Delta x \Delta y} \iint h_c(x - x', y - y') d_c(x', y') dx dy. \quad (5.50)$$

The convolution integral in (5.50) can also be discretized at the nonuniformly sampled input grid, using an appropriate quadrature rule. In order to perform this discretization, the portion of the plane covered by the receivers must be tessellated, i.e. divided in nonoverlapping cells. There are multiple ways to perform this tessellation. Ferber and Özbek use the Delaunay triangulation, also mentioning that Voronoi tessellation could be used instead.

When the Delaunay triangulation is used the tessellation cells are triangles whose vertices are the sampling points (x_i, y_j) . In this case it is convenient to discretize the

integral using the trapezoidal rule. The trapezoidal rule for numerically integrating a function $f(x', y')$ for a triangularly tessellated integration domain is given by

$$\begin{aligned} \int_{0\Delta x}^{N_x\Delta x} \int_{0\Delta y}^{N_y\Delta y} f(x', y') dx' dy' &\approx \sum_{l=0}^{N_T-1} \frac{1}{3} \sum_{\substack{i,j: \\ (x_i, y_j) \in T_l}} f(x_i, y_j) \text{Area}(T_l) = \\ &= \sum_{i=0}^{N_x-1} \sum_{j=0}^{N_y-1} f(x_i, y_j) \sum_{\substack{l: \\ (x_i, y_j) \in T_l}} \frac{1}{3} \text{Area}(T_l), \end{aligned} \quad (5.51)$$

where N_T is the number of triangles and $T_l = ((x_{l1}, y_{l1}), (x_{l2}, y_{l2}), (x_{l3}, y_{l3}))$ is a triangle as generated by the tessellation and is defined by three input grid points that act as its vertices. The area of a particular triangle can be calculated by the determinant of a matrix composed by the coordinates of the vertices

$$\text{Area}(T_l) = \frac{1}{2} \left| \det \begin{pmatrix} x_{l1} & y_{l1} & 1 \\ x_{l2} & y_{l2} & 1 \\ x_{l3} & y_{l3} & 1 \end{pmatrix} \right|. \quad (5.52)$$

In our case $f(x', y') = \frac{1}{\Delta x \Delta y} h_c(x - x', y - y') d_c(x', y')$. Substituting in (5.51) we get

$$d_{\text{GF}}(x, y) \approx \frac{1}{\Delta x \Delta y} \sum_{i=0}^{N_x-1} \sum_{j=0}^{N_y-1} \left[\sum_{l:(x_i, y_j) \in T_l} \frac{1}{3} \text{Area}(T_l) \right] h_c(x - x_i, y - y_j) d(x_i, y_j), \quad (5.53)$$

Note that $d_c(x_i, y_j)$ has been replaced by $d(x_i, y_j)$ since by assumption $d(x, y) = d_c(x, y)$ for $(x, y) = (x_i, y_j)$. Therefore no interpolation has to be performed on the data, it is only the filter that is interpolated. The interpolated filter coefficients are weighted by

$$w_{\text{DEL}}(x_i, y_j) = \sum_{l:(x_i, y_j) \in T_l} \frac{\text{Area}(T_l)}{3\Delta x \Delta y} \quad (5.54)$$

which is 1/3 of the total area covered by cells that have (x_i, y_j) as their common vertex, normalized by the nominal cell area. It can be seen that the value of $w_{\text{DEL}}(x_i, y_j)$ depends purely on geometrical information about the input locations and the kind of tessellation used. It can also be seen that a relatively isolated input location will receive more weight than one that is located in a denser part of the input grid.

When the Voronoi tessellation is used, the tessellation cells are polygons whose generators are the sampling points (x_i, y_j) . Because the vertices of the polygons generally do not coincide with sampling points, it is convenient to discretize the integral using a quadrature rule of the type

$$\int_{0\Delta x}^{N_x\Delta x} \int_{0\Delta y}^{N_y\Delta y} f(x', y') dx' dy' \approx \sum_{i=0}^{N_x-1} \sum_{j=0}^{N_y-1} f(x_i, y_j) \text{Area}(P_{i,j}) \quad (5.55)$$

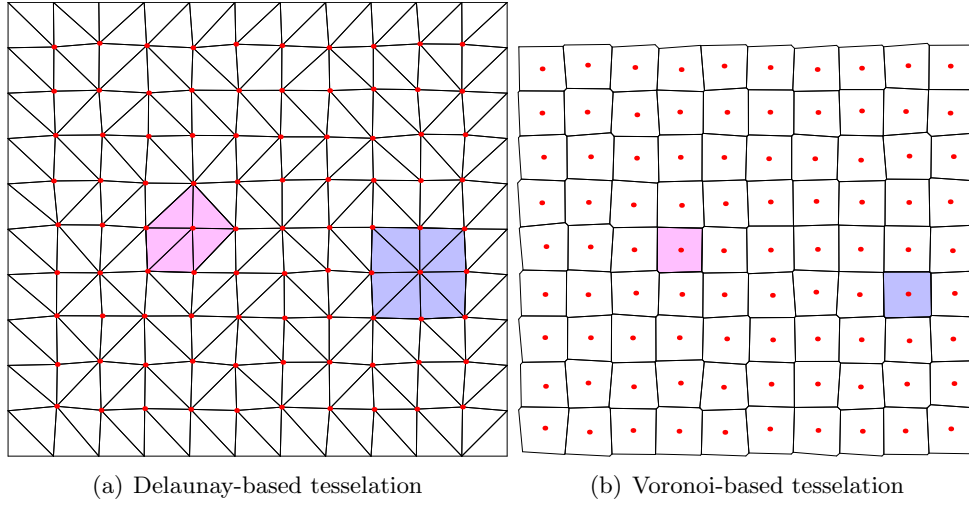


Figure 5.1: Tesselation of the same grid using the Delaunay and Voronoi methods. The cells around the same grid points are highlighted in both tessellations.

where $P_{i,j}$ is the Voronoi cell corresponding to the generator point (x_i, y_j) . Its area can be calculated by dividing the polygon into triangles and using (5.52). Using this quadrature rule, $d_{\text{GF}}(x, y)$ can be approximated as

$$d_{\text{GF}}(x, y) \approx \frac{1}{\Delta x \Delta y} \sum_{i=0}^{N_x-1} \sum_{j=0}^{N_y-1} \text{Area}(P_{i,j}) h_c(x - x_i, y - y_j) d(x_i, y_j). \quad (5.56)$$

The weights of the interpolated filter coefficients are now given by

$$w_{\text{VOR}}(x_i, y_i) = \frac{\text{Area}(P_{i,j})}{\Delta x \Delta y}. \quad (5.57)$$

In Fig. 5.1 examples of the two tessellation methods are shown. Note that if the nominal grid is rectangular the weights that are calculated using the Delaunay triangulation might vary considerably for each input location, even if the input locations have fairly uniform spacings. This happens because the cell around each grid point might contain a different number of triangles (e.g. the pink and blue cells in Figure 5.1(a)). This effect is undesirable since we would like the weight to not vary much when the deviations of the input locations are small. Using the Voronoi tessellation performs better in this respect, generating cells which vary less in area.

After the weights have been determined using any of the tessellation methods, a normalization factor γ is calculated such that

$$\sum_{i=0}^{N_x-1} \sum_{j=0}^{N_y-1} h(i\Delta x, j\Delta y) = \gamma \sum_{i=0}^{N_x-1} \sum_{j=0}^{N_y-1} w_{\{\text{DEL}, \text{VOR}\}}(x_i, y_j) h_c(x_i, y_j). \quad (5.58)$$

Multiplying the weighted filter coefficients by γ has the effect of setting the DC amplitude of the filter to zero. Finally, the discretized convolution can be written as

$$d_{\text{GF}}(x, y) \approx \gamma \sum_{i=0}^{N_x-1} \sum_{j=0}^{N_y-1} w_{\{\text{DEL}, \text{VOR}\}}(x_i, y_j) h_c(x - x_i, y - y_j) d(x_i, y_j) \quad (5.59)$$

5.3.2 The one-dimensional case

In the one-dimensional case tessellation becomes less complicated, as it becomes a problem of dividing a line segment into subsegments. The trapezoidal rule can be used, but now has the form

$$\int_{0\Delta x}^{N_x-1} f(x') dx' \approx \sum_{l=0}^{N_{LS}-1} \frac{1}{2} \sum_{\substack{i: \\ x_i \in LS_l}} f(x_i) \text{Length}(LS_l) = \sum_{i=0}^{N_x-1} f(x_i) \sum_{\substack{l: \\ x_i \in LS_l}} \frac{1}{2} \text{Length}(LS_l), \quad (5.60)$$

where the LS_l are the line segments and N_{LS} is the total number of line segments. In order to approximate the integral, the values of the function $f(x')$ to be integrated have to be known at the input grid points x_i , as well as the length of the subsegments that have x_i in common. Since those subsegments are x_{i-1} to x_i and x_i to x_{i+1} , (5.60) becomes

$$\int_{0\Delta x}^{N_x-1} f(x') dx' \approx \sum_{i=0}^{N_x-1} f(x_i) \frac{1}{2} (x_{i+1} - x_{i-1}). \quad (5.61)$$

The function to be integrated is now $f(x') = h_c(x - x') d_c(x')$, therefore

$$d_{\text{GF}}(x) \approx \sum_{i=0}^{N_x-1} \left[\frac{x_{i+1} - x_{i-1}}{2\Delta x} \right] h_c(x - x_i) d(x_i), \quad (5.62)$$

or

$$d_{\text{GF}}(x) \approx \sum_{i=0}^{N_x-1} w_{LS}(x_i) h_c(x - x_i) d(x_i), \quad (5.63)$$

where $w_{LS}(x_i) = \frac{x_{i+1} - x_{i-1}}{2\Delta x}$.

5.4 Comparison of methods and related discussion

We will now examine more closely the relation of the methods we developed in Section 5.1 with the GCDGF [8] and the band-limited reconstruction method found in [7]. While [7] is concerned with reconstruction rather than group forming, our methods have some conceptual similarities that stem from the band-limited assumption in (5.7).

We begin by examining how a single output of filtered data is generated in each of these methods, for example the output $d_{\text{GF}}(\bar{x}_l)$. In order to make the formulation less cumbersome, we introduce the $N_x \times 1$ vector $\tilde{\mathbf{d}}_{\text{ALL}}$ in which all the acquired data at points x_i , $i = 0, 1, \dots, N_x$ are stacked. We also define the $L_f \times 1$ vector $\tilde{\mathbf{d}}_{\text{PART}}$ that contains those elements of $\tilde{\mathbf{d}}_{\text{ALL}}$ that are within the spatial support of the translated prototype filter $h(\bar{x}_l - x)$. The output value $d_{\text{GF}}(\bar{x}_l)$ can be then calculated using

1. our space domain optimization method. Using (5.17) we have that

$$d_{\text{GF}}(\bar{x}_l) = \underbrace{\text{row}(\mathbf{H}; l)}_{(a)} \underbrace{\tilde{\mathbf{Q}}_l^H (\tilde{\mathbf{Q}}_l \tilde{\mathbf{Q}}_l^H)^{-1}}_{(b)} \underbrace{\tilde{\mathbf{d}}_{\text{PART}}}_{(c)}.$$

Recall that $\tilde{\mathbf{Q}}_l$ is formed by keeping only those rows of \mathbf{Q} that interpolate at the same locations as the data contained in $\tilde{\mathbf{d}}_{\text{PART}}$, therefore it is an $L_f \times N_x$ matrix. We can conceptually interpret the above equation as three distinct operations:

- (a) interpolation of the filter coefficients to the input grid. This is easier to see if $\text{row}(\mathbf{H}; l) \tilde{\mathbf{Q}}_l^H$ is written as $(\tilde{\mathbf{Q}}_l \text{row}(\mathbf{H}; l)^H)^H$. It can be seen that $\tilde{\mathbf{Q}}_l$ acts by interpolating the filter in $\text{row}(\mathbf{H}; l)^H$. The result is then transposed to put the interpolated filter in row form.
 - (b) “deconvolution” of the spectral leakage effects of nonuniform sampling.
 - (c) application of the resulting filter to the nonuniformly sampled data.
2. band-limited reconstruction and traditional filtering. After notation adaptations, (12) from [7] can be written

$$\hat{\mathbf{d}}_{\text{NOM}} = (\mathbf{Q}_R^H \mathbf{W}_D \mathbf{Q}_R + \eta^2 \mathbf{I})^{-1} \mathbf{Q}_R^H \mathbf{W}_D \tilde{\mathbf{d}}_{\text{ALL}}.$$

The vector $\hat{\mathbf{d}}_{\text{NOM}}$ holds the data reconstructed at the nominal grid. The matrix $N_x \times N_x$ matrix \mathbf{Q}_R performs band-limited interpolation from the nominal grid to the input grid, i.e. $\mathbf{d}_{\text{ALL}} = \mathbf{Q}_R \hat{\mathbf{d}}_{\text{NOM}}$. The $N_x \times N_x$ diagonal weighting matrix \mathbf{W}_D and the scalar quantity η^2 are present because of the maximum a posteriori (MAP) regularization used in [7] to deal with missing samples and stability. In order to expose the similarities of this method with our own, we will make the simplifications $\mathbf{W}_D = \mathbf{I}$ and $\eta = 0$, effectively removing the regularization. Then,

$$\begin{aligned} d_{\text{GF}}(\bar{x}_l) &= \text{row}(\mathbf{H}; l) \hat{\mathbf{d}}_{\text{NOM}} \\ &= \underbrace{\text{row}(\mathbf{H}; l)}_{(c)} \underbrace{(\mathbf{Q}_R^H \mathbf{Q}_R)^{-1}}_{(b)} \underbrace{\mathbf{Q}_R^H \tilde{\mathbf{d}}_{\text{ALL}}}_{(a)} \end{aligned}$$

Again three steps can be recognized.

- (a) interpolation of the acquired data to the nominal grid.
 - (b) “deconvolution” of the effects of the spectral leakage effects of nonuniform sampling.
 - (c) application of the prototype filter to the reconstructed data.
3. GCDGF with band-limited interpolation of the filter. Any kind of interpolation can be used with GCDGF, but for the sake of comparison we will assume that

band-limited interpolation will be used to interpolate the filter coefficients to the input grid. Then, the output at \bar{x}_l is given by

$$d_{\text{GF}}(\bar{x}_l) = \underbrace{\text{row}(\mathbf{H}; l) \tilde{\mathbf{Q}}_l^H}_{(a)} \underbrace{\mathbf{W}_C}_{(b)} \underbrace{\tilde{\mathbf{d}}_{\text{PART}}}_{(c)},$$

where \mathbf{W}_C are the geometry compensating weights corresponding to the input data in $\tilde{\mathbf{d}}_{\text{PART}}$. The three steps of this method can be summarized as follows:

- (a) interpolation of the prototype filter coefficients to the input grid.
- (b) sampling density-dependent compensation for nonuniform sampling.
- (c) application of the resulting filter to the nonuniformly sampled data.

We can see that methods 1 and 2 are conceptually similar, but work in “opposite directions”: the first method reconstructs a prototype filter on the input grid, whereas the second reconstructs the data on the nominal grid. An interesting point arises when $L_f = N_x$, that is when the filter $\tilde{\mathbf{g}}_l$ is allowed to have as many taps as the total number of data samples. Then $\tilde{\mathbf{Q}}_l = \mathbf{Q}_R$ and is a square $N_x \times N_x$ matrix. In this special case, $\tilde{\mathbf{Q}}_l^H (\tilde{\mathbf{Q}}_l \tilde{\mathbf{Q}}_l^H)^{-1} = (\mathbf{Q}_R^H \mathbf{Q}_R)^{-1} \mathbf{Q}_R^H$ and both methods give the same result if no regularization is used. An important difference is how these two methods handle the case of missing samples. This means that some output locations might have less than L_f data samples within the support of the prototype filter. The first method will generate a filter $\tilde{\mathbf{g}}_l$ with less than L_f taps. The second method, however, can reconstruct samples, therefore the prototype filter with its L_f taps can be used intact. The quality of the output will of course depend on the quality of the reconstruction. Similarly, the quality of the output of the first method will be limited by the performance of a filter that has less taps than desired.

The first and the third method have a common first step, in that both interpolate a prototype filter to the input grid. The main difference is that GCDGF corrects for sampling density deviations but does not attempt to deconvolve nonuniform sampling effects, which can sometimes lead to reduced performance. On the other hand, because a least-squares problem is not involved, The GCDGF is computationally much cheaper.

6.1 Experimental setup: one-dimensional case

In order to test the performance of the proposed algorithms, a set of synthetic data was created using modeling software based on finite differences numerical methods.

6.1.1 Acquisition geometry and velocity model

Traces are recorded every $\delta x = 1\text{m}$ on the surface along a straight line on the x -axis. The 1m spacing is used to simulate the dense grid. We assume a receiver nominal spacing of $\Delta x = 10\text{m}$ and therefore $M_x = 10$. The deviation δx_i of each receiver is allowed to lie in the interval $[0, \alpha\Delta x]$. For the Figs. 6.5-6.7 the parameter $\alpha = 0.8$. The dense grid point \bar{x}_p closest to the actual receiver location x_i is found and the generated trace at \bar{x}_p is used as the synthetic data trace for the receiver location x_i . The deviations are chosen randomly for each realization of the receiver geometry and are following the uniform distribution. In this way it is possible to simulate nonuniform sampling. In total 2500 traces are generated, which can support $N_x = 250$ receivers and their potential deviations. Each trace is sampled with a sampling interval of $\Delta t = 1\text{ms}$ for a total of $N_t = 1501$ samples per trace. Additive white Gaussian noise was added to the traces so that the overall SNR is 20dB.

The subsurface model is a simple 3 layer model. The first interface has a slight dip and each layer is denser than the previous one. Primary and secondary waves travel with different velocities in each of the layers. The structure is depicted in Fig. 6.1, where the depth, density and supported wave velocities are shown. Each layer is homogeneous.

6.1.2 Source wavelet

The source is located at an offset of 500m, on the x -axis. The wavelet emitted by the source has a duration $T_{\text{wav}} = 0.05\text{s}$. It is given by the second derivative of a Blackman-Harris window and is given by

$$f_{\text{wav}}(t) = 0.48829 \cos\left(\frac{2\pi}{T_{\text{wav}}}t\right) - 0.56512 \cos\left(\frac{2\pi}{T_{\text{wav}}}2t\right) + 0.07683 \cos\left(\frac{2\pi}{T_{\text{wav}}}3t\right)$$

The wavelet can be seen in Fig. 6.2 along with its magnitude and phase spectrum. Its bandwidth is approximately 70Hz and its phase is linear.

6.1.3 Filtering and decimation

We assume that a decimation by a factor $\beta = 3$ will be performed on the data. The spacing of the output values will be $\Delta x' = \beta\Delta x = 30\text{m}$. A FIR filter of length

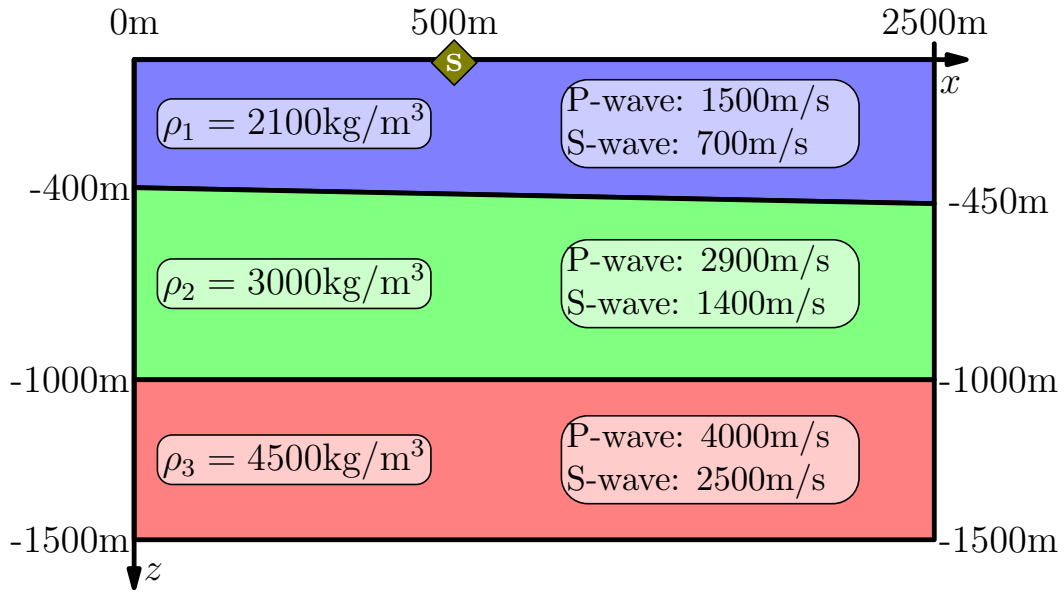


Figure 6.1: A schematic depiction of the velocity model with ρ_i the density of layer i .

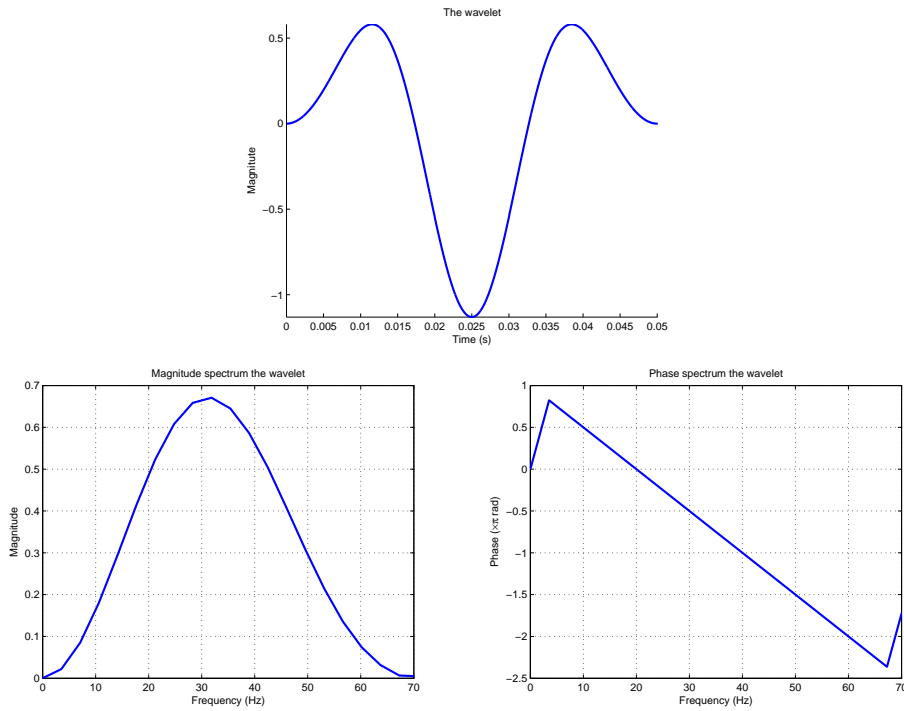


Figure 6.2: The time representation and spectrum of the second derivative of the modified Blackman-Harris window with a duration of 0.05s.

$L_f = 7$ was designed using the least squares method with the passband in $[0, 0.15\pi]$ and the stopband in $[0.25\pi, 1\pi]$ in normalized wavenumbers. This filter works as an anti-alias filter in order to suppress normalized wavenumbers above 0.333π . This filter

is approximated by our spatial domain method and by the geometry compensating digital group forming (GCDGF) algorithm. The bandpass (sinc) interpolation was used to interpolate the filter coefficients.

Our wavenumber domain method tries to approximate an ideal filter with the same passband and stopband. The prototype filter's wavenumber response can be seen in Fig. 6.3. The elements of the $N_x \times N_x$ weighting matrix \mathbf{W} are given below

$$W_{m,n} = \begin{cases} \frac{1}{\delta_p}, & \text{if } |b + m\frac{2\pi}{N_x}| \leq k_{\text{pass}} \\ 0, & \text{if } k_{\text{pass}} < |b + m\frac{2\pi}{N_x}| < k_{\text{stop}} \\ \frac{1}{\delta_s}, & \text{if } |b + m\frac{2\pi}{N_x}| \geq k_{\text{stop}} \end{cases}, \quad (6.1)$$

where $0 \leq m, n \leq N_x - 1$ and

$$b = \begin{cases} -\pi & \text{if } N_x \text{ even} \\ -1 + \frac{1}{N_x} & \text{if } N_x \text{ odd} \end{cases}.$$

For the results in the next subsection, $\delta_p = \delta_s = 0.01$, $k_{\text{pass}} = 0.15\pi$ and $k_{\text{stop}} = 0.25\pi$. The effect of \mathbf{W} , when constructed as per (6.1) is to apply a weight $1/\delta_p$ in the passband and a weight $1/\delta_s$ in the stopband. The zero weight in the in-between wavenumbers effectively removes them from consideration, thus declaring them as a transition band. Note that every row of \mathbf{W} has the same weight. This means that the off-diagonal elements of each row are equally weighted to the diagonal element of that same row.

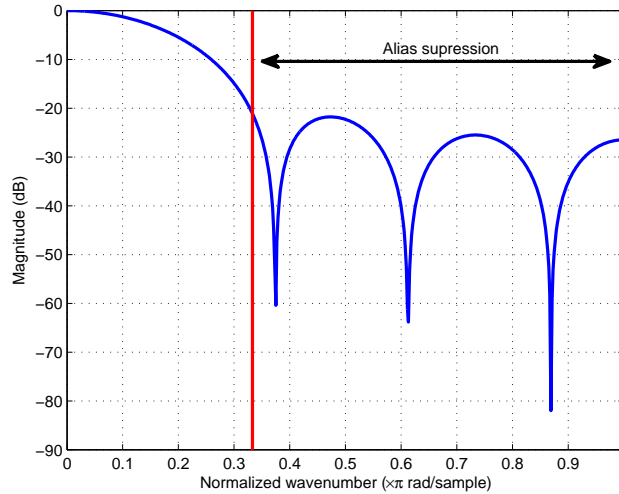


Figure 6.3: The prototype 7 tap filter to be approximated.

6.1.4 Results - one spatial dimension

Before discussing the performance of the algorithms presented in the previous chapters, it is useful to examine the spectrum of the data in the ideal case where no receivers are misplaced. This can be seen in Fig. 6.4(a). The ground roll is much stronger than the reflection energy near $k = 0 \text{ m}^{-1}$. If the data were subject to resampling with the

ground roll left untreated, a significant amount of energy could potentially fold back to the low-wavenumber region.

Applying the filter of Fig. 6.3 to the uniformly sampled data gives the filtered version seen in Fig. 6.4(b). The spectral zeros of the filter can be clearly seen around $\pm 0.038 \text{ m}^{-1}$, $\pm 0.061 \text{ m}^{-1}$ and $\pm 0.09 \text{ m}^{-1}$. As expected, the ground roll energy in the stopband is attenuated, but its portion in the passband is almost left intact. This is because our filter is designed with anti-aliasing in mind and is a wavenumber filter: its passband does not change with frequency¹.

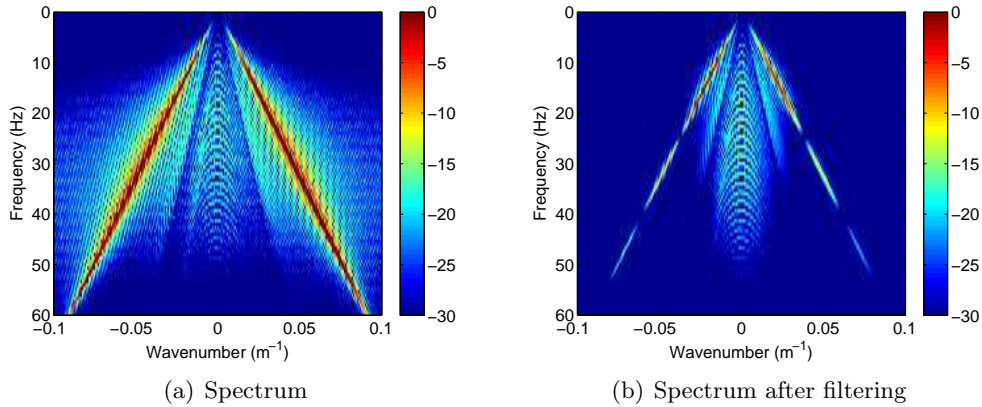


Figure 6.4: The FK spectrum of uniformly sampled data before and after filtering.

When the signal is not uniformly sampled, the situation is more complicated. The average power spectrum of the filtered data can be seen in Fig. 6.5. One plot was generated for each method. It is interesting to see what happens when we apply the prototype filter of Fig. 6.3 to *nonuniformly* sampled data. The average result can be seen in Fig. 6.5(a). The problem of this approach is immediately apparent: although energy in the stopband is suppressed very well, the passband content on average differs considerably from the ideal of Fig. 6.4(b). This confirms what was discussed in Chapter 4, namely that simply ignoring irregularities in the sampling pattern may not give results that are satisfactory. Good performance in the low-wavenumber region is crucial since it holds the energy of the reflection events.

Another interesting fact can be noted in Fig. 6.5(a). In the lower frequencies up to 30Hz, the spectrum of the filtered output is not far from that of Fig. 6.4(b). At first it might seem as if the filter performs better in that region. The truth is that lower wavenumbers are less influenced by irregularities in sampling. The reason can be intuitively understood with a simplified thought experiment. Consider two spatial waves that have the same amplitude but different wavenumbers. The first has a low wavenumber, the second one a high wavenumber. The first wave has a big wavelength and varies very slowly; therefore the error introduced by sampling close to the desired coordinate but not exactly at it does not introduce a big error in the measurement of the wave's amplitude. On the contrary, the high-wavenumber wave will vary more quickly

¹It is possible to use *velocity* filters that attenuate specific velocity bands. We do not examine these kinds of filters in this thesis, but the interested reader can refer to [11].

in amplitude and sampling jitter might give significantly different measurements. What happens in the low frequency region of the spectrum is less vulnerable to sampling jitter for the same reason.

The performance of our two proposed algorithms can be seen in Figs 6.5(b) and 6.5(c). On average they perform better than the previous method. Note that in Figs 6.5(b) the attenuation around the wavenumbers $\pm 0.038 m^{-1}$, $\pm 0.061 m^{-1}$ and $\pm 0.09 m^{-1}$ is not as large as the attenuation seen in Fig. 6.4(b) at the same wavenumbers. The filters designed by the spatial domain method is an approximation of the prototype filter and is not guaranteed to exhibit exactly the same characteristics.

The average power spectrum of the GCDGF can be seen in Fig. 6.5(d). The performance of the one-dimensional GCDGF² is better than the first approach of simply applying the LSI filter directly to the nonuniformly sampled data, but slightly worse than using our proposed methods. GCDGF interpolates the filter to the receiver locations and corrects for sampling density, which leads to better performance than using filter coefficient values calculated for uniformly sampled data. However, as discussed in Section 5.4, it does not attempt to correct for the spectral leakage introduced by the nonuniform sampling. Our proposed methods do, which is why a better result can be achieved.

The standard deviation from the average for each method can be seen in Fig. 6.6. The standard deviation has been normalized to the highest value of the average power spectrum. The standard deviation can be considered as a measure of *robustness* of the algorithms, in the sense that it reveals how much the output spectrum varies when the layout of the receivers on the field varies. Smaller values mean that the output of an algorithm does not vary much for a different realization of the receiver locations. All methods exhibit some variance as would be expected, especially in the passband region. However, our proposed algorithms exhibit a smaller standard deviation since they partially remove the spectral leakage due to nonuniform sampling which is the biggest contributor to the variance of the output.

In Fig. 6.7 the difference of the average power spectra from the ideal output power spectrum of Fig. 6.4(b). It can be seen as a measure of the *accuracy* of the algorithms, as it reveals how close is the output on average to the ideal output. It can be again seen that our proposed algorithms give an output that is very close to the ideal output. The difference is normalized with respect to the highest value of the ideal power spectrum of the output.

6.2 Experimental setup: two-dimensional case

Due to the unavailability of synthetic data created by a more advanced method, such as the finite differences method used for the one-dimensional case, the synthetic data was created using simpler method that employs a superposition of plane waves at the receivers. Also, the author's implementation of the wavenumber domain method for the two-dimensional case proved to be, in practice, extremely demanding in computational power to be used for the following simulations, therefore simulations were performed

²As derived in Section 5.3.

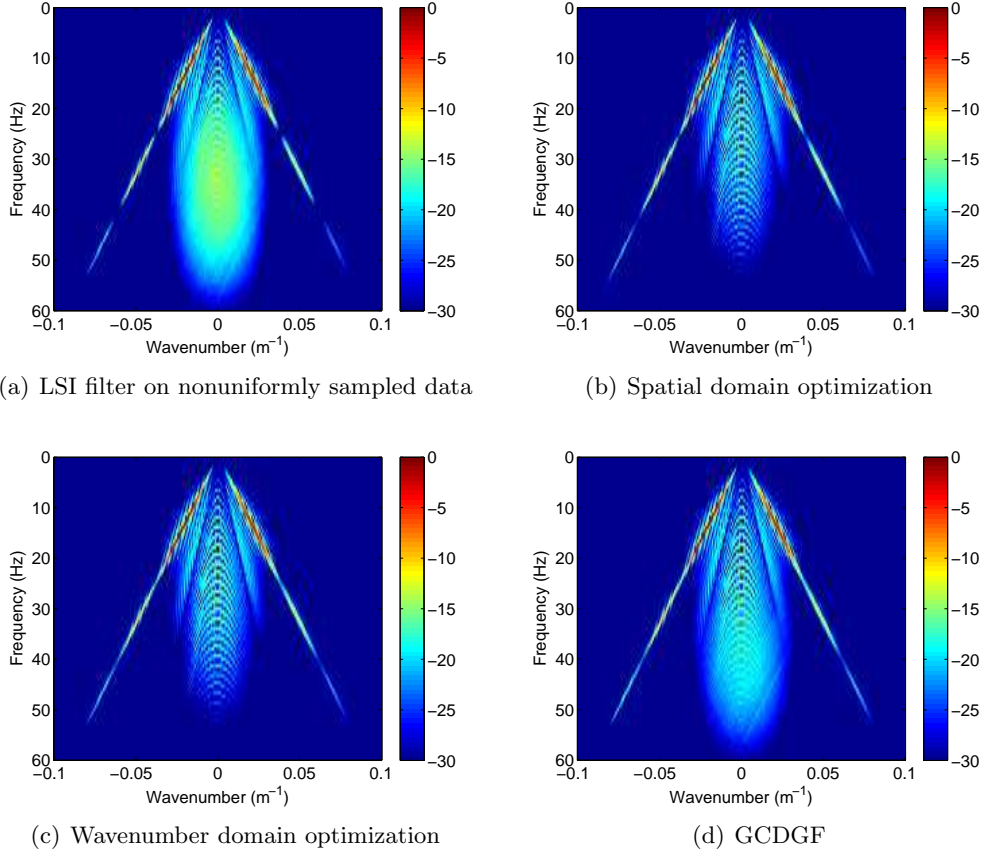


Figure 6.5: The average spectrum of the output.

only for the three other methods.

6.2.1 Acquisition geometry

The traces are generated on a rectangular grid with a sampling interval $\delta x = \delta y = 1.25m$. This grid plays the role of the dense grid. The nominal spacing between the receivers is $\Delta x = \Delta y = 12.5m$. It follows that $M_x = M_y = 10$. The deviation of each receiver along the x -axis, $\delta x_{i,j}$, lies in the interval $[0, \alpha_x \Delta x]$ and $a_x = 0.8$ in our simulations. Similarly, the deviation along the y -axis, $\delta y_{i,j}$, lies in the interval $[0, \alpha_y \Delta y]$ and for the following results, $\alpha_y = 0.8$. Nonuniform sampling is simulated in the same way as the one-dimensional case. The dense grid has 1000×1000 points and covers the area $[0m, 1250m] \times [0m, 1250m]$. $N_x N_y$ receivers are distributed on the dense grid, where $N_x = N_y = 100$. Each trace contains $N_t = 150$ time samples, with a sampling interval of $\Delta t = 0.01s$.

6.2.2 Generating the data

As mentioned earlier, the data was generated using a superposition of plane waves that arrive at the receivers. The plane waves are generated by N_s sources. For our simulation

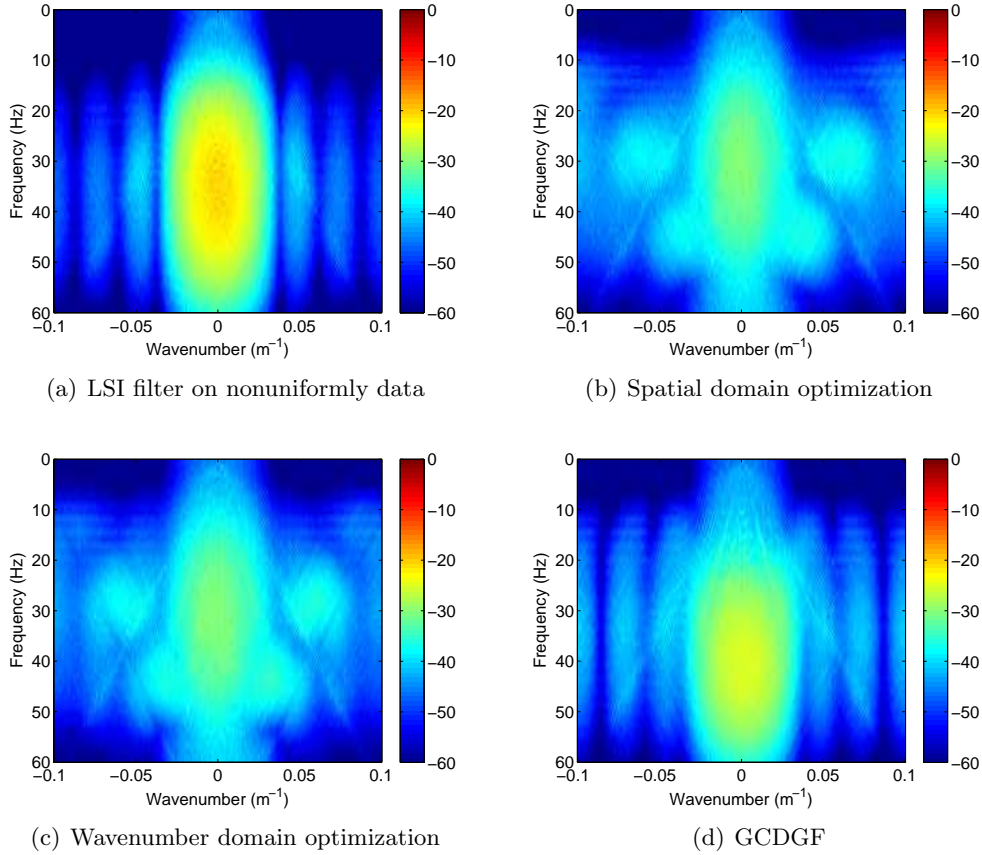


Figure 6.6: Standard deviation from the average output spectrum.

we use $N_s = 2$ sources: one at $(x_{s1}, y_{s1}, z_{s1}) = (500m, 500m, 0m)$ which is on the same plane ($z = 0$) as the receivers and simulates the ground roll. The apparent velocity of the ground roll is $c_1 = 1200m/s$. This value is too high to be realistic. It was used here to prevent severe aliasing of the ground roll. Each source generates plane waves with frequencies in a certain range. For the ground roll this range is $\phi_1 = [1Hz, 45Hz]$.

The second source simulates the reflections coming from beneath and is placed at the location $(x_{s2}, y_{s2}, z_{s2}) = (500m, 500m, 3000m)$. The apparent velocity of the plane waves generated by this source is $c_2 = 2000m/s$ and the frequency range is again $\phi_2 = [1Hz, 45Hz]$.

The data is generated at the frequency-space domain and is given by

$$d(f, x, y) = \sum_{\substack{1 \leq l \leq N_s \\ l: f \in \phi_l}} \frac{1}{\sqrt{R_l(x, y)}} e^{-i2\pi f(R_l(x, y)/c_l)} \quad (6.2)$$

where $R_l(x, y) = \sqrt{(x_{sl} - x)^2 + (y_{sl} - y)^2 + z_{sl}^2}$ is the distance between the l th source and the receiver at $(x, y, 0)$. In our case we evaluate $d(f, x, y)$ at the grid points of the dense grid and at N_t equispaced frequencies in the range $[-\frac{1}{2\Delta t}, \frac{1}{2\Delta t}]$. Then the data in time can be recovered by means of an inverse DFT. Before the inverse transform is

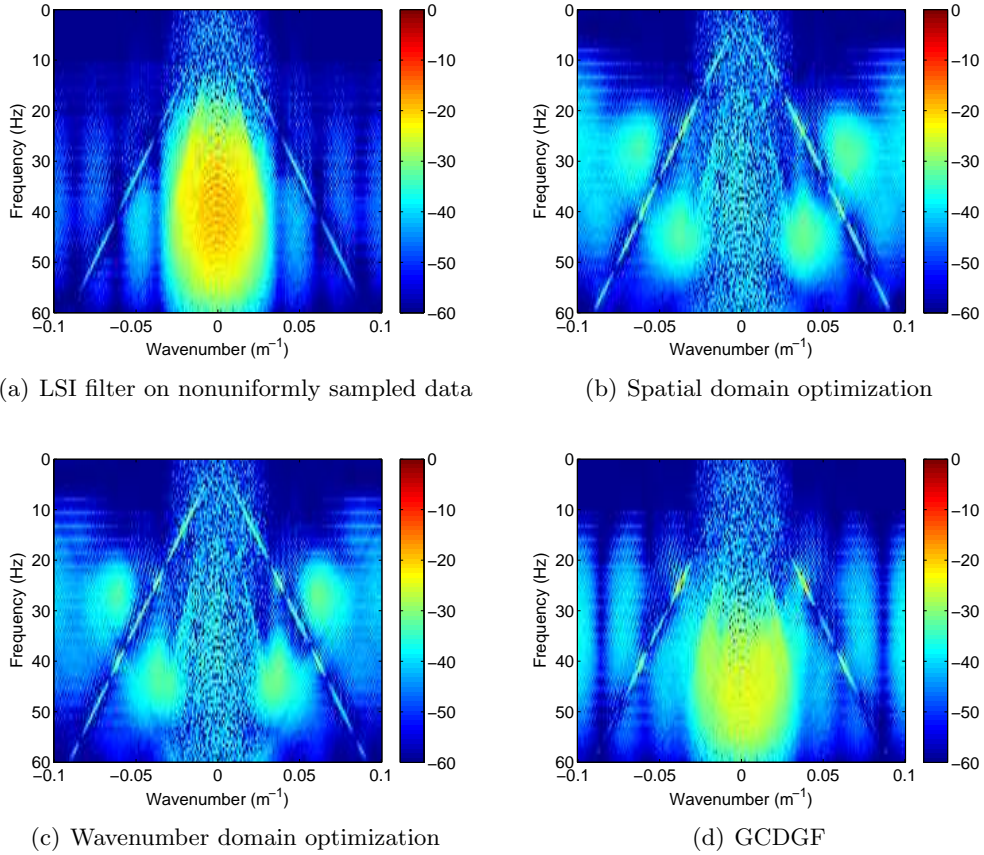


Figure 6.7: Difference of the average output spectrum from the ideal of Fig. 6.4(b).

applied, a window is applied along the frequency axis in order to minimize the ringing effect caused by sharp boundaries. A Blackman-Harris window was used in our case.

6.2.3 Filtering and decimation

Similar to the one-dimensional case, we use a predesigned FIR filter as an input to our spatial domain method. The filter is again designed for the same antialiasing scenario as in the one dimensional case. The difference is that this time the filter is two-dimensional and is approximately circularly symmetric. This is a desired property since plane waves arriving at any apparent angle experience the same attenuation. The filter used here is a Gaussian lowpass filter designed using the window method. The filter lengths are $L_{fx} = L_{fy} = 9$ and its cutoff is at the normalized wavenumber 0.3π . The magnitude of its wavenumber response can be seen in Fig. 6.2.3.

6.2.4 Results - two spatial dimensions

We begin by first examining the spectral content of the data that will be filtered. This can be found in Fig. 6.9(a). It is a “frequency-wavenumber-wavenumber” (FKK) plot where each slice shows the spectral content along the two wavenumber axes k_x and k_y

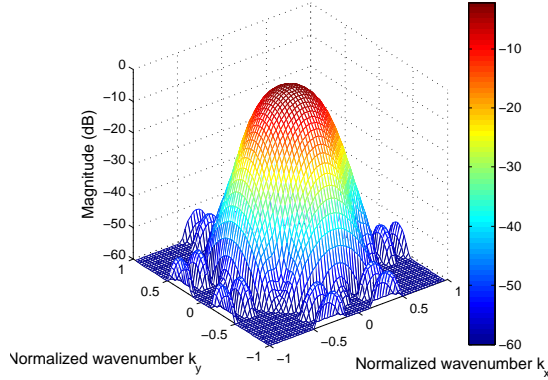


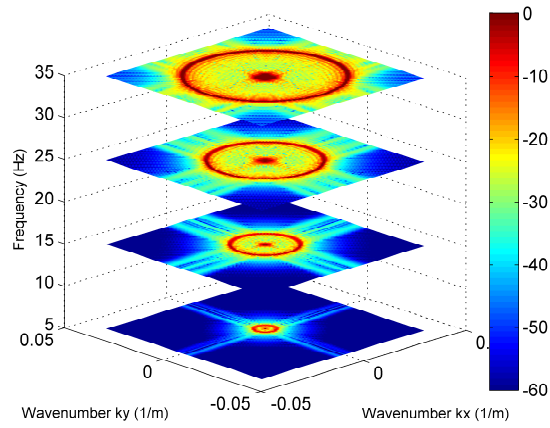
Figure 6.8: The two-dimensional FIR filter.

for a given frequency³. The reflection energy is concentrated near $k_x = k_y = 0m^{-1}$ and does not expand much for higher frequencies. The ground roll, on the other hand, appears as a sequence of expanding rings in each slice, due to its lower velocity. This is analogous to the one-dimensional case.

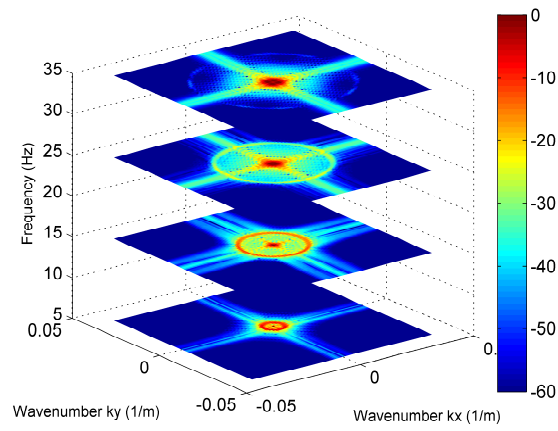
When the circularly symmetric filter is applied to the uniformly sampled data, the resulting spectrum is seen in Fig. 6.9(b). Both the reflection energy and the ground roll are within the passband region for $f = 5Hz$ and $f = 15Hz$. For $f = 25Hz$ we notice that the ground roll starts entering the stopband region of the filter and gets attenuated. For $f = 35Hz$, the ground roll has practically been suppressed.

The same types of plots as the one-dimensional case were generated in order to evaluate the performance of each method. The results found on Figs. 6.10 - 6.12 were calculated over 20 different realizations of the receiver locations, for each one of the methods. Checking the average output spectra of Fig. 6.10 for each of the methods, we can see that they are in general close to the ideal one of Fig. 6.9(a). However, the our spatial domain method gives an average result that is less accurate in the passband, a fact which can be seen clearly in Fig. 6.12(b). Fig. 6.12(b) shows the difference between the ideal output of Fig. 6.9(b) and the average spectrum of the output of the spatial domain method. This is not anticipated, as it is completely opposite from what was seen in the one-dimensional case, where the spatial domain method generally exhibits a better performance in the passband than the other methods. This discrepancy is a strong indicator that the implementation of the spatial domain method for the two-dimensional case and/or the simulation setup have to be further scrutinized for mistakes.

³Note that the frequency axis in the two-dimensional case is reversed compared to the one-dimensional case results, for the ease of depiction.

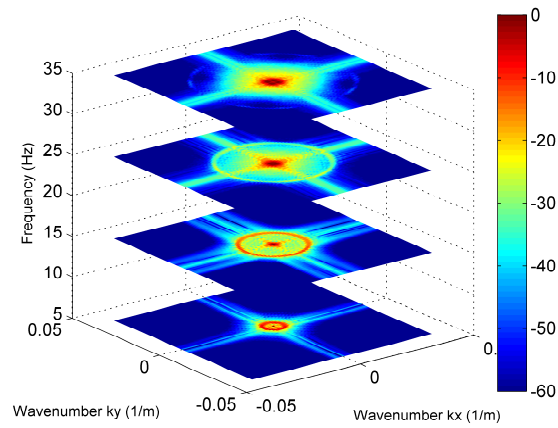


(a) Spectrum

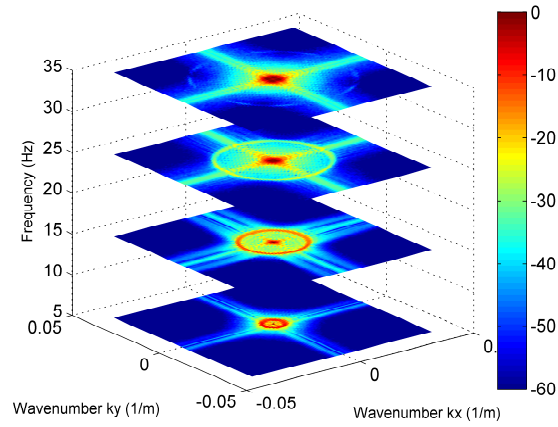


(b) Spectrum after filtering

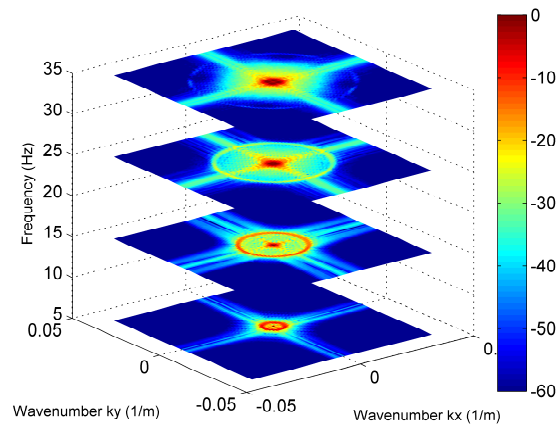
Figure 6.9: The FKK spectrum of uniformly sampled data before and after filtering.



(a) LSI filter on nonuniformly sampled data

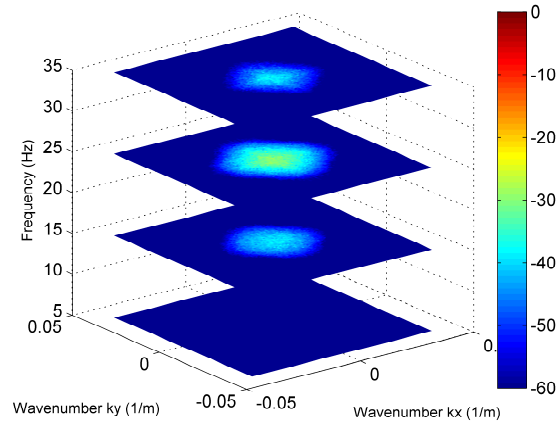


(b) Spatial domain optimization

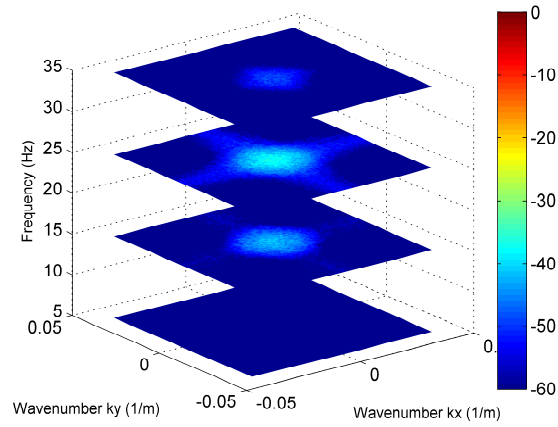


(c) GCDGF

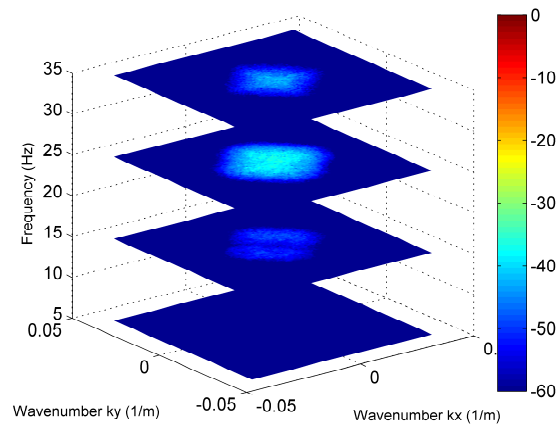
Figure 6.10: The average spectrum of the output.



(a) LSI filter on nonuniformly sampled data

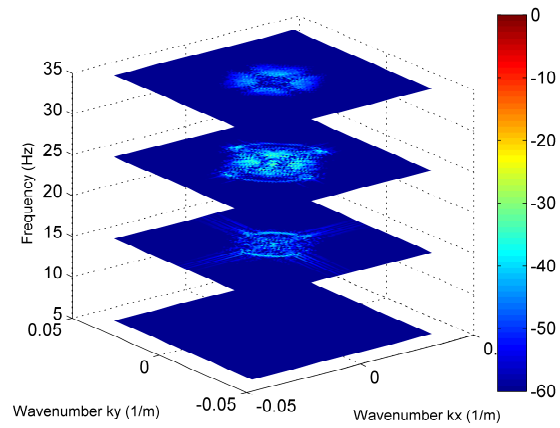


(b) Spatial domain optimization

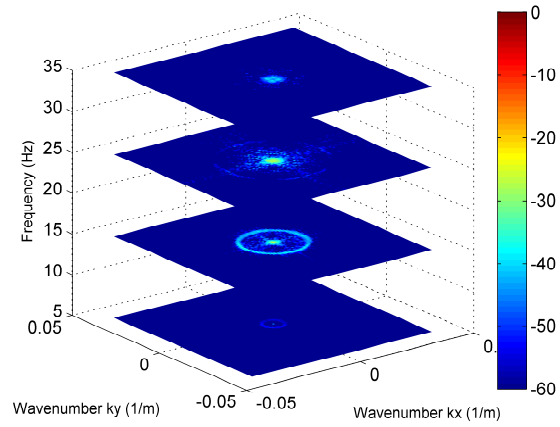


(c) GCDGF

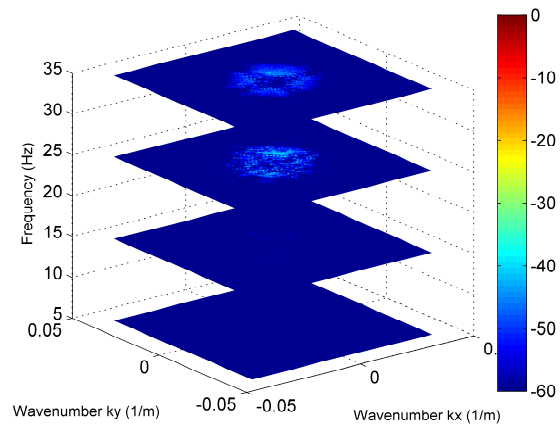
Figure 6.11: Standard deviation from the average output spectrum.



(a) LSI filter on nonuniformly sampled data



(b) Spatial domain optimization



(c) GCDGF

Figure 6.12: Difference of the average output from the ideal of Fig. 6.9

Conclusions and suggestions for future work

7

This thesis began by examining the relation of the spectral content of the data captured by the seismic receivers to the apparent velocity of arriving wavefronts. It was then discussed how the problems of data volume reduction, SNR improvement and spectral content suppression have been traditionally dealt with by summing the output of multiple receivers arranged in arrays with a specific geometric layout. New advances in seismic acquisition hardware permit single sensor recording which enables digital group forming, which is a way that enables digital array forming. Conceptually, group forming can be thought of as a filtering operation on the data, followed by a resampling operation. It was shown that misplacements of receivers introduce a form of spectral leakage to the data that may make a simple filtering operation an unsatisfactory solution for the first step of group forming.

Two methods were proposed to deal with this problem. Both of them design a LSV filter that can be used to filter the data. This LSV filter acts as an anti-aliasing filter and generates outputs that lie on the nominal grid. The difference between the two proposed methods is that the first approximates a predesigned LSI filter defined in the spatial domain, while the second approximates the ideal filter defined in the wavenumber domain. The first method gives us the ability to approximate filters that may be designed using any filter design algorithm. The second method, on the other hand, also incorporates the filter design method in its formulation. Our first proposed method shares conceptual similarities with other methods proposed in the bibliography, as well as a number of differences. One of these alternative methods, GCDGF, is examined in closer detail and a version of it, suitable for one-dimensional spatial data is derived.

The methods were implemented and tested on synthetic data. In the case of sampling jitter that follows the uniform distribution and when no receivers are missing, the proposed methods for the one-dimensional case exhibit, on average, are more robust and accurate in filtering than both GCDGF and simply applying an LSI filter on the nonuniformly sampled data. The reason behind this performance is the fact that our proposed algorithms compensate for the spectral smearing introduced by irregularities in sampling. On the other hand, the proposed algorithms are computationally more expensive than GCDGF due to the fact that a least squares optimization problem has to be solved. When the receiver locations only have very small perturbations, it may be possible to get acceptable results at much less time by ignoring the sampling irregularities.

Unfortunately the same conclusions could not be verified for the two-dimensional case, as the performance of the spatial domain algorithm was not at par with the performance of the one-dimensional version of the algorithm. For the wavenumber domain method, the computational complexity is an important issue that has to be tackled before the algorithm can be used on real data.

This work introduces a number of possible topics for further discussion and research.

- The LSV filter designed by the methods introduced in Chapter 5 generates filter outputs on the nominal grid. However, many times resampling is also desired. The possibility of generating outputs on an arbitrary grid could be investigated.
- A way to construct the weighting matrix \mathbf{W} is given in Section 6.1.3. This is not the only possibility however and is not necessarily the best.
- Assess the performance of the algorithms when the data contains gaps.
- Implement a computationally efficient algorithm for the wavenumber optimization method.

Appendix



A.1 The sincd() function

The full proof for the formula of the sincd(\cdot) function will be given below. We differentiate between two cases depending on whether N_x is odd or even. In both cases the proof is conceptually the same: the data sampled on the nominal grid is transformed to the wavenumber domain, followed by an inverse transform evaluated on the dense grid.

Let N_x be odd and P be an integer such that $N_x = 2P + 1$. The forward DFT of $d(\bar{x}_q)$ is given by

$$D_{\text{DFT}}(p) = \sum_{q=0}^{N_x-1} d(\bar{x}_q) e^{-\iota \frac{2\pi}{N_x \Delta x} p \bar{x}_q} \Delta x, \quad p = -P, -P+1, \dots, P \quad (\text{A.1})$$

The inverse DFT evaluated at the locations \bar{x}_n is given by

$$d(\bar{x}_n) = \frac{1}{N_x \Delta x} \sum_{p=-P}^P D_{\text{DFT}}(p) e^{\iota \frac{2\pi}{N_x \Delta x} p \bar{x}_n}, \quad n = 0, 1, \dots, N_x M_x - 1 \quad (\text{A.2})$$

Substituting (A.1) in (A.2) we get

$$d(\bar{x}_n) = \frac{1}{N_x \Delta x} \sum_{p=-P}^P \left(\sum_{q=0}^{N_x-1} d(\bar{x}_q) e^{-\iota \frac{2\pi}{N_x \Delta x} p \bar{x}_q} \Delta x \right) e^{\iota \frac{2\pi}{N_x \Delta x} p \bar{x}_n} \quad (\text{A.3})$$

After exchanging the order of the summations we get

$$d(\bar{x}_n) = \sum_{q=0}^{N_x-1} \frac{1}{N_x} d(\bar{x}_q) \left(\sum_{p=-P}^P e^{\iota \frac{2\pi}{N_x \Delta x} p (\bar{x}_n - \bar{x}_q)} \right) \quad (\text{A.4})$$

The term in the parentheses is a geometric series and can be rewritten in closed-form

$$d(\bar{x}_n) = \sum_{q=0}^{N_x-1} \frac{1}{N_x} d(\bar{x}_q) \left(\frac{e^{\iota \frac{2\pi}{N_x \Delta x} (-P) (\bar{x}_n - \bar{x}_q)} - e^{\iota \frac{2\pi}{N_x \Delta x} (P+1) (\bar{x}_n - \bar{x}_q)}}{1 - e^{\iota \frac{2\pi}{N_x \Delta x} (\bar{x}_n - \bar{x}_q)}} \right) \quad (\text{A.5})$$

Multiplying the nominator and denominator with $e^{\iota \frac{2\pi}{N_x \Delta x} (-\frac{1}{2}) (\bar{x}_n - \bar{x}_q)}$ and applying the Euler formula we get

$$d(\bar{x}_n) = \sum_{q=0}^{N_x-1} d(\bar{x}_q) \underbrace{\frac{\sin(\frac{\pi}{\Delta x} (\bar{x}_n - \bar{x}_q))}{N_x \sin(\frac{\pi}{N_x \Delta x} (\bar{x}_n - \bar{x}_q))}}_{\text{sincd}(N_x; \bar{x}_n, \bar{x}_q), N_x \text{ odd}}. \quad (\text{A.6})$$

When N_x is even, a slight complication arises. The index p takes values $-P+1, -P+2, \dots, P$, where $2P = N_x$. The forward DFT now contains the Nyquist wavenumber for $p = P$. In order for the interpolator to be real, three strategies can be followed. The first is to omit the Nyquist wavenumber and the second is to duplicate it. Both of these strategies guarantee that the imaginary part of the Nyquist wavenumber vanishes. The third strategy is to multiply the Nyquist wavenumber with $1/2$ and then duplicate it. Yaroslavsky argues in [19] that the third strategy decays faster to zero, thus introducing less boundary effects. The $\text{sincd}()$ function for the even N_x case can be obtained with a modification of (A.4)

$$d(\bar{x}_n) = \sum_{q=0}^{N_x-1} \frac{1}{N_x} d(\bar{x}_q) \left(\sum_{p=-P+1}^{P-1} e^{i \frac{2\pi}{N_x \Delta x} p (\bar{x}_n - \bar{x}_q)} + \frac{1}{2} \left(e^{i \frac{2\pi}{N_x \Delta x} (-P) (\bar{x}_n - \bar{x}_q)} + e^{i \frac{2\pi}{N_x \Delta x} P (\bar{x}_n - \bar{x}_q)} \right) \right).$$

Using similar steps as before, we arrive at

$$d(\bar{x}_n) = \sum_{q=0}^{N_x-1} d(\bar{x}_q) \underbrace{\left(\frac{\sin\left(\frac{(N_x-1)\pi}{N_x \Delta x} (\bar{x}_n - \bar{x}_q)\right)}{N_x \sin\left(\frac{\pi}{N_x \Delta x} (\bar{x}_n - \bar{x}_q)\right)} + \frac{1}{N_x} \cos\left(\frac{\pi}{\Delta x} (\bar{x}_n - \bar{x}_q)\right) \right)}_{\text{sincd}(N_x; \bar{x}_n, \bar{x}_q), N_x \text{ even}}. \quad (\text{A.7})$$

Using the L'Hôpital rule, it is easy to see that when $\bar{x}_n = \bar{x}_q$, $\text{sincd}(N_x; \bar{x}_n, \bar{x}_q) = 1$.

Bibliography

- [1] GJM Baeten, VJM Belougne, MJM Daly, BJM Jeffryes, and JE Martin. Acquisition and processing of point source measurements in land seismic. In *2000 SEG Annual Meeting*, 2000.
- [2] F.J. Beutler and O.A.Z. Leneman. The spectral analysis of impulse processes. *Information and Control*, 12(3):236–258, 1968.
- [3] Ronald E Crochiere and Lawrence R Rabiner. *Multirate digital signal processing*. 1983.
- [4] P.J. Davis. *Circulant matrices*. Chelsea Publishing Company, 1994.
- [5] M.A.Z. Dippé and E.H. Wold. Antialiasing through stochastic sampling. In *ACM SIGGRAPH Computer Graphics*, volume 19, pages 69–78. ACM, 1985.
- [6] B. Dragoset. A historical reflection on reflections. *The Leading Edge*, 24:S46–S71, 2005.
- [7] AJW Duijndam, MA Schonewille, and COH Hindriks. Reconstruction of band-limited signals, irregularly sampled along one spatial direction. *Geophysics*, 64(2):524–538, 1999.
- [8] R. Ferber and A. Ozbek. Method and apparatus for filtering irregularly sampled data, June 3 2008. US Patent 7,382,685.
- [9] M.H. Hayes. *Statistical digital signal processing and modeling*. John Wiley & Sons, 2009.
- [10] M. Holzman. Chebyshev optimized geophone arrays. *Geophysics*, 28(2):145–155, 1963.
- [11] ER Kanasewich. *Time series sequence analysis in geophysics*, 1981.
- [12] F. Marvasti. *Nonuniform sampling: theory and practice*. Springer, 2001.
- [13] L. Ongkiehong. A changing philosophy in seismic data acquisition. *First break*, 6(9):281–284, 1988.
- [14] Alan V Oppenheim, Ronald W Schafer, John R Buck, et al. *Discrete-time signal processing*, volume 2. Prentice hall Englewood Cliffs, NJ:, 1989.
- [15] JO Parr and WH Mayne. A new method of pattern shooting. *Geophysics*, 20(3):539–564, 1955.
- [16] C.H. Savit, J.T. Brustad, and J. Sider. The moveout filter. *Geophysics*, 23(1):1–25, 1958.
- [17] M. Schoenberger. Optimization and implementation of marine seismic arrays. *Geophysics*, 35(6):1038–1053, 1970.

- [18] G.J.O. Vermeer. *Seismic wavefield sampling: a wave number approach to acquisition fundamentals*, volume 4. Society of Exploration Geophysicists, 1990.
- [19] LP Yaroslavsky. Efficient algorithm for discrete sinc interpolation. *Applied optics*, 36(2):460–463, 1997.